CHARACTERIZATION OF SEMICONDUCTORS BY ELECTRON BEAM INDUCED CURRENT

BY

TAKASHI FUYUKI

JANUARY 1981

DEPARTMENT OF ELECTRONICS

KYOTO UNIVERSITY

KYOTO, JAPAN

CHARACTERIZATION OF SEMICONDUCTORS
BY
ELECTRON BEAM INDUCED CURRENT

BY

TAKASHI FUYUKI

JANUARY 1981

DEPARTMENT OF ELECTRONICS

KYOTO UNIVERSITY

KYOTO, JAPAN

ABSTRACT

The electron beam induced current (EBIC) was analyzed quantitatively considering the three-dimensional generation distribution by an electron beam. The solutions of the steady-state or time-dependent diffusion equations assuming a point source can be applied to the case of the finite generation distribution by the dividing method. The EBIC was found to be affected very much by the generation distribution the extent of which was comparable with the minority carrier diffusion length. In the line scan method, the dependence of EBIC on the scanning distance represents mainly the lateral extent of the generation distribution. The three-dimensional generation distribution was clarified combining the normal incidence and the line scan methods of EBIC. The improved method to measure the diffusion length and the surface recombination velocity was suggested.

The minority carrier distribution is influenced very much by the sample dimensions when they are equal to or smaller than the diffusion length. The EBIC was analyzed by a simple method using an image source-and-sink distribution. The EBIC was found to be dependent on the surface recombination velocity and the sample dimensions rather than the diffusion length.

The lifetime and the diffusion constant of minority carriers could be determined definitely without any restriction of modulation frequency by the phase shift technique using EBIC.

The improved method to measure the diffusion length was applied to the heat treatment effect in Si. The diffusion length was found to be decreased very much after the heat treatment at 1000 °C for only a few minutes.

The physical properties such as the diffusion length in the small selected areas could be characterized by EBIC considering the three-dimensional generation distribution by an electron beam and the sample dimensions. Experimental results in Si and GaAs showed good agreement with the theory, and the generation distributions in Si and GaAs were revealed with experiments.

ACKNOWLEDGEMENTS

The author wishes to express his deep gratitude to former Professor Tetsuro Tanaka for his continuing guidance and grateful encouragement. The author wishes to express his greatful appreciation to Associate Professor Hiroyuki Matsunami for his precious guidance and helpful advice throughout the present study. The author acknowledges Professor Akira Kawabata for his genial guidance and encouragement. The author is greatful to Professor Toshinori Takagi for his stimulating discussions and useful criticisms on the manuscript. The author would also like to thank Professor Akio Sasaki for a critical reading of the manuscript and valuable comments.

Much attention is due to Dr. Junji Saraie, Dr. Shigehiro Nishino and Dr. Akira Suzuki for their continuous encouragement and stimulative discussions.

The author thanks other members of Semiconductor Laboratory for their considerable assistance and experimental facilities.

CONTENTS

LIST OF SYMBOLS

c	correction factor with which the three-dimensional solutions of the gradient of phase shift can be expressed by the one-dimensional approximations
C	exponent of Gaussian distribution
d_g	position of generation source from the surface along the depth
D	diffusion constant of minority carriers
D_g	($\equiv d_g/L$) normalized generation depth
e	charge of an electron
E_{pc}	electron-hole pair creation energy by an electron beam
f	modulation frequency of primary electron beam
g	generation rate of actual point source
Δg	variable part of generation source
G	the whole generation strength in the generation region
i	imaginary unit
I_B	primary electron beam current
I_{EBIC}	measured electron beam induced current
I_L	current which flows through the load resistance
I_0	backward saturation current
I_{SC}	short circuit current
j	electron beam induced current
$\bar{j}^*$	variable part of complex electron beam induced current
J	($=\eta$) normalized electron beam induced current; it becomes unity when all the generated carriers contribute to electron beam induced current.
J^*	normalized electron beam induced current considering the influence of ohmic contact

k	correction factor for the incident beam energy considering the energy loss due to backscattered electrons
$\frac{kT}{e}$	thermal voltage; =25.9 mV at room temperature
K_1	second-modified first-order Bessel function
L	diffusion length of minority carriers
L^*	diffusion length estimated directly from the slope of electron beam induced current vs. scanning distance curve
L^{**}	diffusion length estimated directly from the slope of electron beam induced current vs. scanning distance curve considering the influence of ohmic contact
L^*_{eff}	$(\equiv L/\sqrt{1+i\omega\tau})$ complex effective diffusion length
p	distribution of minority carrier density
p^*	distribution of minority carrier density considering the influence of ohmic contact
$\bar{p}^*$	variable part of the distribution of minority carrier density; complex variable
r	distance between the center of the generation region and each divided segment
R	radius of generation region
R_c	center of generation region
R_e	extraporated electron range
R_L	load resistance
R_m	maximum electron range
s	surface recombination velocity
S	$(\equiv s/(L/\tau))$ surface recombination velocity parameter
t	time
T	variable for integration
u	parameter for Gaussian distribution
V_a	accelerating voltage of primary electron beam

w	distance between the potential barrier and the ohmic contact
w_d	depletion layer width
w_m	metal thickness of Schottky diode
x	Cartesian co-ordinate of scanning distance
X	$(\equiv x/L)$
x_g	distance between the potential barrier and the generation point along the scanning direction
X_g	$(\equiv x_g/L)$
y	Cartesian co-ordinate on the scanning surface normal to the scanning direction
z	Cartesian co-ordinate along the depth
z_m	peak of the Gaussian distribution

η	$(=J)$ collection efficiency
$\Delta\eta$	collection efficiency of the variable part of the generation source
ρ	resistivity of semiconductors
ρ_{Au}	mass density of Au; $=18.9\ g/cm^3$
ρ_{GaAs}	mass density of GaAs; $=5.3\ g/cm^3$
ρ_{Si}	mass density of Si; $=2.3\ g/cm^3$
τ	minority carrier lifetime
ϕ	phase shift between the electron beam induced current and the modulated generation source
Φ	diameter of primary electron beam
ω	angular frequency of modulated primary electron beam

I. INTRODUCTION

The remarkable progress in the solid state devices is owing to the advancement in the characterization technique of the device materials. When the devices having new functions are developed, the detail knowledge of the physical properties of the semiconducting material (bandgap, lifetime and mobility of carriers, etc.) must be needed. In particular, those properties must be characterized after the actual manufacturing process, because the original properties may be affected by the various process conditions.

In recent years, to characterize very small devices (i.e. LSI's or laser diodes), there has been a growing interest to use a finely focused electron beam. The two dimensional information of the material properties can be obtained non-destructively with high spatial resolution from the electron beam interaction with samples [1,2]. Surface morphology can be observed with great depth of focus by a scanning electron microscope (SEM). Crystal defects in thin samples are detected using a scanning electron transmission microscope (STEM) [3,4]. A scanning Auger electron microscope (SAM) [5] has become a very useful tool to analyze the surface and the interface region.

The method using an electron beam induced current (EBIC)[6-10] is a very convenient technique to determine the fundamental parameters (e.g. the diffusion length, the lifetime and the surface recombination velocity of minority carriers) which control the electrical performance of the devices. The electron-hole pairs generated by an electron beam are seperated by the internal field in p-n junctions or Schottky barriers, and the current is induced in the external circuit. The EBIC depends very much on diffusion and recombination of minority carriers in semiconductors, and the diffusion length, etc. can be

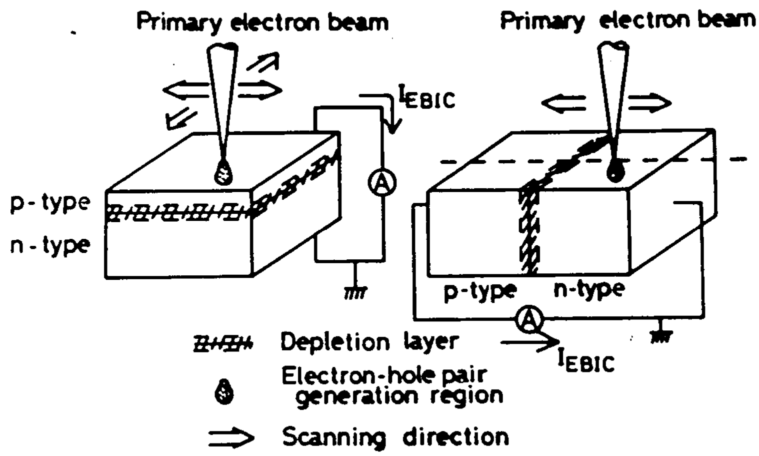

(A) (B)

Fig. 1-1 Principal configurations to measure the electron beam induced current (EBIC).

(A) normal incidence method

(B) line scan method

determined from the analysis of EBIC. In addition to the two dimensional information of the diffusion length and the lifetime, their variations along the depth can be obtained for various generation depths by changing the accelerating voltage of an electron beam.

The principal configurations to measure EBIC are the 'normal incidence method' and the 'line scan method' (see Fig. 1-1). In the normal incidence method, the electron beam is incident normal to the barrier plane and is scanned on the surface parallel to that plane. The dislocations and defects in Si were observed in p-n junctions and Schottky barrier diodes [11-28]. In recent years, electrical activity of oxidation induced stacking faults (OSF's) and its relation with device performances have been studied [29-35]. The normal incidence method is also used for the failure analysis of the MOS devices [36-39]. Using the line scan method, the diffusion length and the surface recombination velocity can be determined from the dependence of EBIC on the scanning distance when the electron beam is scanned across the barrier. There have been many theoretical [40-46] and experimental [47-69] reports to measure the diffusion length and the surface recombination velocity in light-emitting diodes (LED's) and laser diodes.

In almost all the works so far, EBIC has been analyzed only qualitatively or semi-quantitatively. The diffusion length and the surface recombination velocity have been determined under rather special conditions as mentioned below for the simple theoretical calculation. In the normal incidence method, they considered only the one-dimensional generation distribution along the depth [70-75] under the configuration that the lateral extent of the generation volume was very small compared with sample areas. In the line scan method, the generation volume was assumed to be a point [53,54,60,61] under the condition that the generation volume was sufficiently smaller than the diffusion length and the sample dimensions. But, in the actual case, the generation volume has a finite three-dimensional extent related to the accelerating voltage [76-78]. The latest microelectronic devices (i.e. LSI's and the laser diodes, etc.) have the same dimensions as the generation volume, and so, the analyses considering the point source or the one-dimensional generation distribution are inaccurate to determine the diffusion length and the surface recombination velocity. The new method for the quantitative analysis of EBIC must be developed taking the three-dimensional generation distribution and the influences of the sample dimensions into account [79,80].

In the present study, EBIC is analyzed quantitatively by solving the steady-state or time-dependent three-dimensional diffusion equations. The influence of the finite generation volume on EBIC is discussed when the extent of the generation volume cannot be ignored, and improved methods are suggested to measure the physical properties (diffusion length, lifetime and surface recombination velocity of minority carriers, electron-hole pair creation energy by an electron beam, etc.) in the small selected areas.

In Chapter II, various models for the generation distribution along the depth [77, 81-83] are compared with each other, and the influence of the generation distribution on the determination of the diffusion length by the normal incidence method is discussed.

Chapter III shows the influence of the generation volume on EBIC in the line scan method taking the surface recombination effect into account. An improved method for the determination of the diffusion length and the surface recombination velocity is described.

In Chapter IV , three-dimensional generation distribution is clarified by measuring EBIC using both the normal incidence and the line scan methods in the same sample, which yields the quantitative analysis of EBIC.

Chapter V describes the influence of the sample dimensions on EBIC. In the line scan method, EBIC is investigated by extending the mirror image method [41-43] when the diffusion length is of the order of the sample dimensions.

In Chapter VI , the phase shift technique in the measurement of EBIC [84-86] is described. The relation between the lifetime and the phase shift is clarified by solving the three-dimensional time-dependent diffusion equation. The lifetime and the diffusion constant of minority carriers can be determined combining the phase shift technique with the conventional line scan method.

Chapter VII shows the heat treatment effect on the diffusion length in Si.

Finally, conclusions and suggestions for further investigation are summarized in Chapter VIII .

Experimental results in Si and GaAs are shown in every chapter. The method discussed in these chapters can be applied easily to any semiconductor materials by considering the physical properties inherent in the materials.

References

[1] V. E. Johnson: †SEM /1975/ p.763

[2] O. C. Wells; SEM /1972/ p.375

[3] P. M. Petroff, D. V. Lang, J. L. Strudel and R. A. Logan: SEM /1978/ pp.325-332

[4] C. E. Lyman: SEM /1978/ pp.529-536

[5] N. C. McDonald: SEM /1971/ p.89

[6] D. B. Holt: "Quantitative Scanning Electron Microscopy " (D. B. Holt et al. eds. Academic Press, 1974) pp.213-286

[7] D. B. Wittry: "Microprobe Analysis" (C. A. Anderson ed. John Wiley & Sons, New York, 1973) pp.123-187

[8] C.J.Varker: "Nondestructive Evaluation of Semiconductor Materials and Devices" (ed. Jay N. Zemel, NATO ADVANCED STUDY INSTITUTES SERIES, SERIES B: Physics vol. 46 PLENUM PRESS, 1979) pp.515-580

[9] H. J. Leamy, L. C. Kimerling and S. D. Ferris: SEM /1978/ pp.717-725

[10] The bibliography on EBIC is listed in the following.
K. O. Leedy: Solid State Technology Feb. 1977 pp.45-48

---

†SEM /19xx/ : " Scanning Electron Microscopy " Proceeding of Annual Conference

before 1977 (IIT Research Institute, Chicago)
after 1978 (SEM Inc., AMF O'Hare)

[11] J. J. Lander, H. Schreiber Jr., T.M.Buck and J. R. Mathews: Appl. Phys. Lett. 3 , 206-207 (1963)

[12] W. Czaja and G. H. Wheatley : J. Appl. Phys. 35 , 2782-2783 (1964)

[13] W. Czaja and J. R. Patel : J. Appl. Phys. 36 , 1476-1482 (1965)

[14] N. F. B. Neve and P. R. Thornton: Solid-State Electron. 9 , 900-901 (1966)

[15] I. G. Davies, K. A. Hughes, D. V. Sulway and P. R. Thornton: Solid-State Electron. 9 , 275-279 (1966)

[16] W. Czaja: J. Appl. Phys. 37 , 918-919 (1966)

[17] D. V. Sulway, P. R. Thornton and M. J. Turner: Soli-State Electron. 11 , 567-568 (1968)

[18] A. J. R. Kock, S. D. Ferris, L. C. Kimerling and H. J. Leamy: Appl. Phys. Lett. 27 , 313-315 (1975)

[19] D. B. Holt and R. Ogden: Solid-State Electron. 19 ,37-40(1976)

[20] H. J. Leamy, L. C. Kimerling and S. D. Ferris: SEM /1976/ pp.529-538

[21] T. Kato, T. Matsukawa and R. Shimizu: Appl. Phys. Lett. 26 , 415-416 (1975)

[22] R. B. Marcus, M. Robinson, T. T. Sheng, S. E. Haszko and S. P. Murarka: J. Electrochem. Soc. 124 , 425-430 (1977)

[23] L. C. Kimerling, H. J. Leamy and J. R. Patel: Appl. Phys. Lett. 30 , 217-219 (1977)

[24] D. E. Ioannou and S. M. Davidson: phys. stat. sol. (a) 48 , K1-K4 (1978)

[25] H. Blumtritt, R. Gleichmann, J. Heydenderich and H. Johansen: phys. stat. sol. (a) 55 , 611-620 (1979)

[26] H. Menniger, H. Raidt and R. Gleichmann: phys. stat. sol. (a) 58 , 173-180 (1980)

[27] P. Ashburn and C. J. Bull: Solid-State Electron. 22 , 105-110 (1979)

[28] P. Ashburn, C. J. Bull and J. R. A. Beale: J. Appl. Phys. 50 , 3472-3477 (1979)

[29] K. V. Ravi, C. J. Varker and C. E. Volk: J. Electrochem. Soc. 120 , 533-541 (1973)

[30] C. J. Varker and K. V. Ravi: J. Appl. Phys. 45,272-287 (1974)

[31] S. Kawado, Y. Hayafuji and T. Adachi: Jpn. J. Appl. Phys. 14 , 407-408 (1975)

[32] T. E. Seidel, S. E. Haszko and D. M. Maher: J. Appl. Phys. 48 , 5038-5042 (1977)

[33] A. Murgai, J. Y. Chi and H. C. Gatos: J. Electrochem. Soc. 127 , 1182-1186 (1980)

[34] S. Kawado: Jpn. J. Appl. Phys. 19 , 1591-1602 (1980)

[35] J. M. Dishman, S. E. Haszko, R. B. Marcus, S. P. Murarka and T. T. Sheng: J. Appl. Phys. 50 , 2689-2696 (1979)

[36] J. L. Gates and O. K. Griffith: Appl. Phys. Lett. 27 , 43-45 (1975)

[37] J. F. Katalano: SEM /1976/ pp.521-528

[38] P. Roitman and W. R. Bottoms: SEM /1977/ pp.731-738

[39] C. L. Wilson: Solid-State Electron. 23 , 345-356 (1980)

[40] W. H. Hackett Jr.:J. Appl. Phys. 43 , 1649-1654 (1972)

[41] F. Berz and H. K. Kuiken: Solid-State Electron. 19 , 437-445 (1976)

[42] C. van Opdorp: Philips Res. Rept. 32 , 192-249 (1977)

[43] O. von Roos: Solid-State Electron. 21 , 1063-1067 (1978)

[44] O. von Roos: Solid-State Electron. 21 , 1069-1077 (1978)

[45] O. von Roos: Solid-State Electron. 22 , 113-114 and 773-778 (1979)

[46] W. van Roosbroeck: J. Appl. Phys. 26 , 380-391 (1955)

[47] D. B. Wittry and D. F. Kyser: J. Appl. Phys. 36 ,1387-1389 (1965)

[48] H. Higuchi and H. Tamura: Jpn. J. Appl. Phys. 4 , 316-317 (1965)

[49] Yu. P. Demidov, R. P. Gurova, Yu. M. Kushnir, A. I. Frimer and D. V. Fetisov: Sov. Phys. -Semicond. 1 ,1030-1035 (1968)

[50] K. Maeda, A. Kasami, M. Toyama and N. Wakamatsu: Jpn. J. Appl. Phys. 8 , 65-75 (1969)

[51] Zh. I. Alferov, V. M. Andreev, V. I. Korol'kov and V. I. Stremin: Sov. Phys.-Semicond. 4 , 1113-1116 (1971)

[52] C. J. Hwang, S. E. Haszko and A. A. Bergh: J. Appl. Phys. 42 , 5117-5119 (1971)

[53] W. H. Hackett Jr., R. H. Saul, R. W. Dixon and G. W. Kammlott: J. Appl. Phys. 43 , 2857-2868 (1972)

[54] W. Zimmermann: phys. stat. sol. (a) 12 , 671-678 (1972)

[55] M. Aven, J. Z. Devine, R. B. Bolon and G. W. Ludwig: J. Appl. Phys. 43 , 4136-4142 (1972)

[56] G. Lidgard: Solid-State Electron. 15 , 159-164 (1972)

[57] D. B. Holt, B. D. Chase and M. Censlive;
phys. stat. sol. (a) 20 , 459-467 (1973)

[58] D. B. Holt and B. D. Chase; phys. stat. sol. (a) 20 ,
135-144 (1973)

[59] C. van Opdorp, R. C. Peters and M. Klerk:
Appl. Phys. Lett. 24 , 125-126 (1974)

[60] L. J. Balk, E. Kubalek and E. Menzel:
IEEE Trans. ED-22 . 707-712 (1975)

[61] L. Jastrzebski, J. Lagowski and H. C. Gatos:
Appl. Phys. Lett. 27 , 537-539 (1975)

[62] L. J. Balk, E. Kubalek and E. Menzel: SEM /1975/ pp.447-455

[63] J. J. Oakes, I. G. Greenfield and D. L. Partain:
J. Appl. Phys. 48 , 2548-2555 (1977)

[64] M. Lanir, A. H. B. Vanderwyck and C. C. Wang:
J. Appl. Phys. 49 , 6182-6184 (1978)

[65] D. L. Partain, A. G. Milnes and L. F. Vassamillet:
J. Electrochem. Soc. 126 , 1584-1588 (1979)

[66] N. Tohge, T. Minami and M. Tanaka:
Jpn. J. Appl. Phys. 17 , 2155-2156 (1978)

[67] D. L. Partain, A. G. Milnes and L. F. Vassamillet:
J. Electronic Materials 8 , 493-499 (1979)

[68] D. E. Ioannou and S. M. Davidson:
J. Phys. D: Appl. Phys. 12 , 1339-1344 (1979)

[69] Sheng S. Li, W. L. Wang, P. W. Lai and R. T. Owen:
J. Electronic Materials 9 , 335-354 (1980)

[70] J. F. Bresse: SEM /1972/ pp.105-112

[71] J. F. Bresse: SEM /1977/ pp.683-693

[72] C. J. Wu and D. B. Wittry; J. Appl. Phys. 49, 2827-2836 (1978)

[73] G. E. Possin: SEM /1979/ pp.245-256

[74] G. E. Possin and C. G. Kirkpatrick: J. Appl. Phys. 50 , 4033-4041 (1979)

[75] G. E. Possin and C. G. Kirkpatrick: J. Vac. Sci. Technol. 16 , 1917-1920 (1979)

[76] Von A. E. Gruen: Z. Naturforsch. 12a Heft2 89-95 (1957)

[77] K. Kanaya and S. Okayama: J. Phys. D:Appl. Phys. 5 , 43-58 (1972)

[78] R. Shimizu, Y. Kataoka, T. Ikuta, T. Koshikawa and H. Hashimoto: J. Phys. D:Appl. Phys. 9 , 101-114 (1976)

[79] G. V. Spivak, G. V. Saparin and L. F. Komolova: SEM /1977/ pp.191-199

[80] C. Donolato and H. Klann: J. Appl. Phys. 51 , 1624-1633 (1980)

[81] D. B. Wittry and D. F. Kyser: J. Appl. Phys. 38 , 375-382 (1967)

[82] T. E. Everhart and P.H. Hoff: J. Appl. Phys. 42 , 5837-5846 (1971)

[83] V. V. Makarov: Sov. Phys.-Semicond. 9 , 722-724 (1975)

[84] J. D. Kamm and H. Bernt:Solid-State Electron. 21,957-964(1978)

[85] J. D. Kamm:"Semiconductor Silicon /1977" (J. Electrochemical Society) pp.491-501

[86] O. von Roos: J. Appl. Phys. 50 ,3738-3742 (1979)

II. INFLUENCE OF MINORITY CARRIER GENERATION DISTRIBUTION ON ELECTRON BEAM INDUCED CURRENT IN THE NORMAL INCIDENCE METHOD

2-1. Introduction

Accurate determination of minority carrier diffusion length L is very important to characterize semiconductors. One of the convenient methods to measure L is the use of electron beam induced current (EBIC). The electron-hole pairs generated by an electron beam are seperated by a potential barrier (e.g. p-n junction or Schottky barrier), and the current is induced in the external circuit. The value of L can be determined from the dependence of EBIC on the length z between the potential barrier and the generation point. In the normal incidence method, z is varied by changing the accelerating voltage V_a of an electron beam, and the small value of L of the order of μm can be determined. The value of L in the small region is obtained using a focused beam generated by a scanning electron microscope (SEM).

Czaja [1] measured L in p-n diodes of Si and GaP. He assumed the generation distribution as a combination of two exponential functions. Bresse [2] and Wu [3] measured L and the electron-hole pair creation energy E_{pc} in Si and GaAs. They used Schottky diodes because the electron beam entered through the metal contact, and the surface recombination effect could be neglected. In their analyses, Bresse used the semi-spherical generation distribution proposed by Kanaya et al. [4], and Wu assumed Gaussian distribution. Possin et al. [5] analyzed EBIC in detail taking the influences of the surface recombination and the internal field,

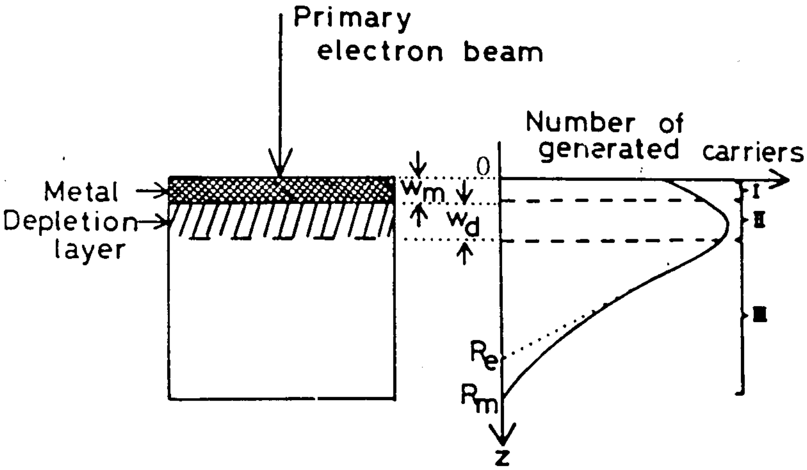

Fig. 2-1 Schematic view of experimental conditions using Schottky diodes. Metal thickness is w_m, and depletion layer width is w_d. The right-hand illustration shows the depth dose function; R_m and R_e give the maximum and extraporated electron range, respectively.

and estimated the depth distribution of lifetime in ion-implanted Si. They used the polynomial function derived by Everhart [6] for the generation distribution.

In the analysis of EBIC, the minority carrier generation distribution plays an important role to determine the accurate value of L and E_{pc}. However, the distribution models used in the analyses are different with each other as mentioned above. In this chapter, we compare various models for the generation distribution in GaAs and Si. We calculate EBIC and clarify the influence of the generation distribution on the determination of L and E_{pc}. Experimental results are also presented.

2-2. Determination of diffusion length and electron-hole pair creation energy

A Schottky barrier diode is used in order to neglect the influence of the surface recombination. The electron beam is irradiated normally to the barrier plane through the metal as shown in Fig. 2-1. The thickness of the metal and the depletion layer are put as w_m and w_d, respectively. The minority carrier generation distribution along the depth (so called the depth dose function) is illustrated also in Fig. 2-1. The EBIC is calculated based on the following assumptions. 1) The minority carriers generated in the metal (region I) cannot contribute to EBIC. 2) The electron-hole pairs generated in the depletion layer (region II) are seperated quickly by the field of the depletion layer, and wholly contribute to EBIC. 3) The minority carriers generated in the bulk (region III) partly contribute to EBIC, i.e. the minority carriers which reach to the edge of the depletion

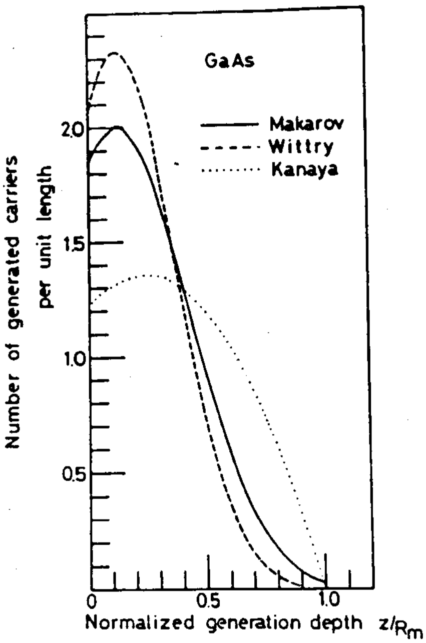

Fig. 2-2

Generation distribution in GaAs. The Makarov's, Wittry's and Kanaya's models are expressed by the solid, broken and dotted lines, respectively. The generation depth is normalized by the maximum electron range R_m. The total generation rate is normalized to be unity.

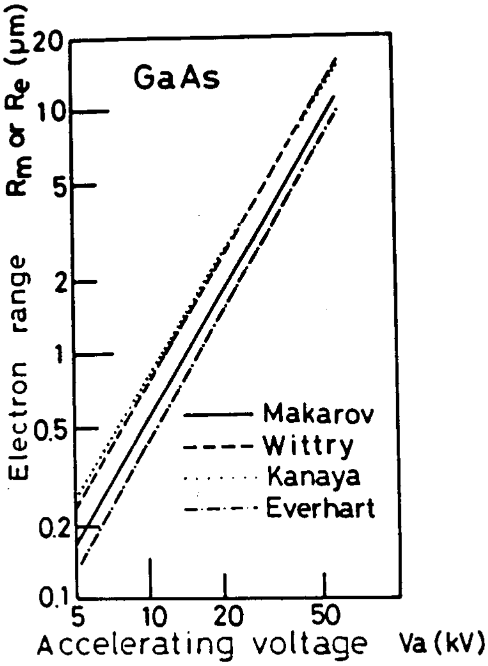

Fig. 2-3

Electron ranges in GaAs for various models. The solid, broken, dotted, and dashed and dotted lines are the results using Makarov's, Wittry's, Kanaya's and Everhart's models, respectively.

layer ($z=w_m+w_d$ in Fig. 2-1) by diffusion can flow into the metal by the field of the depletion layer.

There have been many theoretical [4,7] and experimental [6,8-11] works on the generation distribution. Kanaya and Okayama [4] proposed a semi-spherical generation distribution using the modified diffusion model of Archard [7]. Wittry et al. assumed Gaussian distribution and applied to GaAs [8,9]. Everhart and Hoff [6] derived a polynomial function from their experiments in the Al-SiO_2-Si system. Makarov [10] showed that the generation distribution could be expressed as Gaussian like ($\exp(-((z-z_m)/u)^2)$), and the parameters z_m and u varied according to the atomic number and the density of the material. In order to compare these distributions, normalized depth dose function was introduced. Gruen [11] showed that the shape of the depth dose curve is practically invariant if the penetration depth is normalized by the electron range.

The depth dose function in GaAs normalized by the maximum electron range R_m (at which no electron enters into the material, see Fig. 2-1) are shown in Fig. 2-2 by the solid, broken and dotted lines using the following equations for the models of Makarov, Wittry and Kanaya, respectively.

$$g(z) = \exp\left(-\left(\frac{z/R_m-0.138}{0.43}\right)^2\right) \qquad \text{(Makarov)}, \qquad (2\text{-}1)$$

$$g(z) = \exp\left(-\left(\frac{z/R_m-0.125}{0.35}\right)^2\right) \qquad \text{(Wittry)}, \qquad (2\text{-}2)$$

$$g(z) = (R_m-0.242\ R_m)^2 - (z-0.242\ R_m)^2 \quad \text{(Kanaya)}, \qquad (2\text{-}3)$$

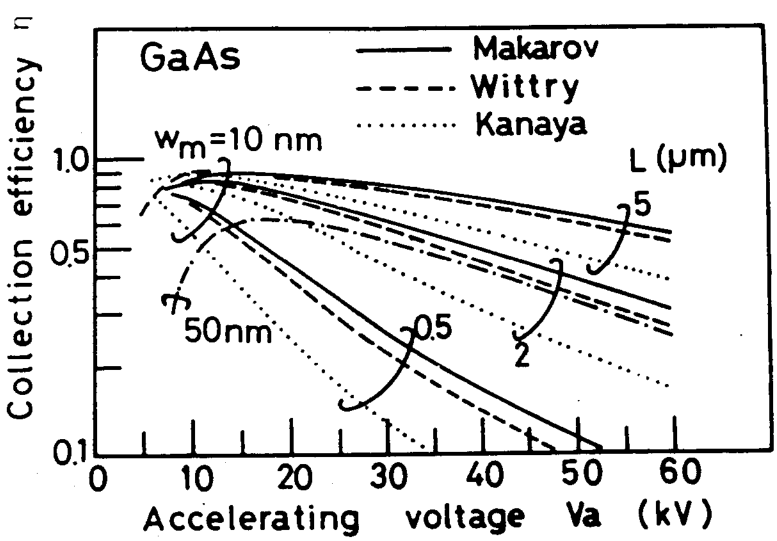

Fig. 2-4 Collection efficiency η vs. V_a curves for GaAs Schottky diode. The values of L are 5, 2 and 0.5 μm from upper to lower group of curves, respectively. The results using the Makarov's, Wittry's and Kanaya's models are expressed by the solid, broken and dotted lines, respectively. The values of w_m and w_d are 10 nm and 0.15 μm, respectively. The dashed and dotted line is in the case of w_m=50 nm, w_d=0.15 μm and L=2 μm using the Wittry's model.

There are obvious differences between these three models. The Makarov's and Wittry's models have the large surface concentration, but the peak value at $z/R_m \approx 0.13$ of the Makarov's model is smaller than that of the Wittry's model. The Kanaya's model has more evenly spreaded distribution than the other two models. This is because the electron-hole pair concentration is assumed to be uniform in the semi-sphere in the Kanaya's model which is a simple first-order approximation for the generation distribution. But, in the actual case, the electron-hole pairs are concentrated around the center of the semi-sphere. One must use the improved electron-hole pair concentration model instead of the uniform one in order to express the generation distribution precisely.

In the calculation of EBIC, the absolute value of R_m must be needed. Some reported values by Makarov, Wittry and Kanaya are shown by the solid, broken and dotted lines, respectively, in Fig. 2-3 for GaAs. The dashed and dotted line is derived by Everhart [6] and discussed later. The ranges of the Wittry's and Kanaya's models are almost agree with each other, but that of the Makarov's model is about 70 % of those of the Wittry's and Kanaya's models.

The calculated EBIC in GaAs (i.e. the collection efficiency η which becomes unity when all the generated carriers contribute to EBIC) by the same method described in ref.[3] is shown in Fig. 2-4. The solid, broken and dotted lines are for the models of Makarov, Wittry and Kanaya, respectively. The value of the accelerating voltage V_a is changed from 5 to 60 kV. The value of L is 5.0, 2.0 and 0.5 μm from upper to lower group of the curves, respectively. The values of w_m and w_d are taken as typical values of 10 nm and 0.15 μm, respectively. The electron range is inversely proportional to the density of the material. The metal thickness is corrected

taking the difference of the densities between the metal and the bulk semiconductor in order that the sample has uniform density from the surface to the bulk for a simple theoretical calculation. When gold is taken as the Schottky contact, w_m must be multiplied by ρ_{Au}/ρ_{GaAs} (=3.6, ρ_{Au}=18.9 and ρ_{GaAs}=5.3 g/cm^3). One can estimate L mainly from the gradient of the curve because the gradient decreases monotonously with increasing L up to 5 μm. The estimated values of L by Makarov's and Wittry's models are almost equal because the gradients of the curves agree with each other for the same L value. The value of L larger than 5 μm cannot be determined definitely because EBIC hardly changes with V_a even if L becomes large. The maximum value of L that can be determined definitely increases as the highest value of V_a increases, but another problems (i.e. damages of the sample by high energy electrons, etc.) may occur. The electron-hole pair creation energy E_{pc} can be obtained from the absolute value of EBIC by the relation $\eta=E_{pc}I_{EBIC}/kI_BV_a$ (I_{EBIC}: measured EBIC, I_B:primary beam current, k:correction factor for the energy loss due to backscattered electrons) [3] .
The absolute values of the Makarov's model are about 10 ∿ 20 % larger than those of the Wittry's model. And so, the value of E_{pc} obtained by the former is 10 ∿ 20 % larger than that by the latter. The gradients and the absolute values of the curves of the Kanaya's model are quite different from those by two other models. The reason of the difference is owing to the assumption of the uniform concentration of the electron-hole pairs in the semi-sphere as discussed before. The Kanaya's model is a first-order approximation for the generation distribution, and is not suitable for the accurate determination of L and E_{pc}. The value of w_d does not affect EBIC so much from the results of the calculation. If w_m becomes large, the absolute value of EBIC at low V_a is decreased very much,

but the gradient of the curve in the region of high V_a does not change as shown in Fig. 2-4 (the dashed and dotted line is in the case of w_m=50 nm, w_d=0.15 μm and L=2 μm using the Wittry's model). Therefore, L can be determined in any case of w_m, as far as w_m is sufficiently small in order that the electron beam can enter into the bulk region.

The normalized depth dose functions in Si expressed by the following equations are shown in Fig. 2-5 by the solid, broken, dotted, and dashed and dotted lines for the models of Makarov, Wittry, Kanaya and Everhart, respectively.

$$g(z) = \exp\left(-\left(\frac{z/R_m - 0.261}{0.37}\right)^2\right) \qquad \text{(Makarov)} \qquad (2\text{-}4)$$

$$g(z) = \exp\left(-\left(\frac{z/R_m - 0.156}{0.44}\right)^2\right) \qquad \text{(Wittry)} \qquad (2\text{-}5)$$

$$g(z) = (R_m - 0.336\ R_m)^2 - (z - 0.336\ R_m)^2 \qquad \text{(Kanaya)} \qquad (2\text{-}6)$$

$$g(z) = 0.6 + 6.21\ z/R_e - 12.40\ (z/R_e)^2 + 5.69\ (z/R_e)^3 \qquad \text{(Everhart)} \qquad (2\text{-}7)$$

Makarov showed that the parameters z_m and u had voltage dependences, and the typical values at V_a=30 kV are taken. It should be noted that the depth dose function of the Everhart's model is normalized by the extraporated range R_e (see Fig. 2-1) which is determined by extraporating the straight line portion of the curve.

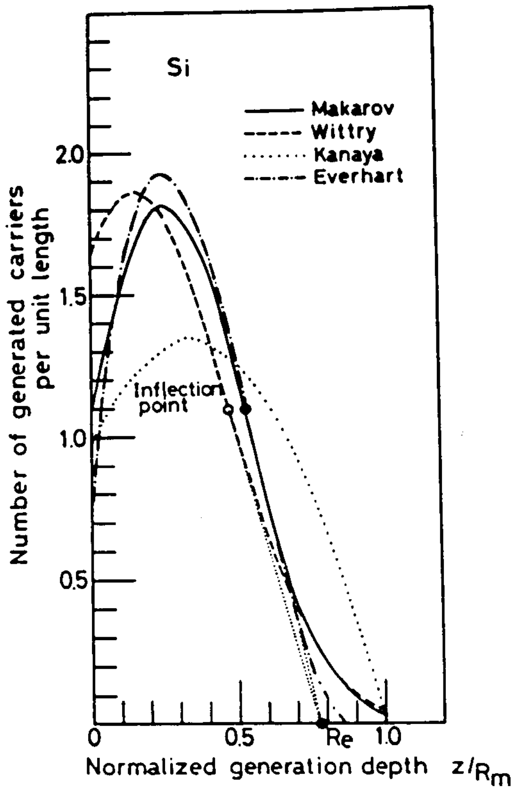

Fig. 2-5 Generation distributions in Si. The Makarov's, Wittry's, Kanaya's and Everhart's models are expressed by the solid,broken, dotted, and dashed and dotted lines, respectively. The generation depth is normalized by the maximum electron range R_m. The extraporated ranges R_e's of the Makarov's, Wittry's and Everhart's models are taken to be agreed with each other. The total generation rate is normalized to be unity.

In order to compare the Everhart's model with others, the extraporated range for the Gaussian distribution is deduced (see footnote)†,and the extraporated ranges of the Makarov's, Wittry's and Everhart's models are taken to be agreed with each other. The peak values of the generation distributions of the Makarov's, Wittry's and Everhart's models are almost equal, but the value of z/R_m at the peak for the Wittry's model is about 0.15 and smaller than those of the other two models ($z/R_m \simeq 0.25$). The generation distribution of the Wittry's model comes nearer to the surface than those of the Makarov's and Everhart's models. It is because the Wittry's model is derived in the case of GaAs, and on the other hand, the Makarov's and Everhart's models are concerned in the case of Si. The density of GaAs (ρ_{GaAs}=5.3 g/cm^3) is larger than that of Si (ρ_{Si}=2.3 g/cm^3), and so, the Wittry's model shows the more surface concentration than the others. The Kanaya's model is quite different with the other three models owing to the same reason as discussed in GaAs.

- - - - - - - - - - - - - - - - - - -

† Gaussian distribution ($\exp(-((z-z_m)/u)^2)$) shows the almost linear decrease around the point of inflection ($z=u/\sqrt{2} + z_m$). The extraporated range R_e (i.e. the point with which the straight line at the point of inflection crosses the z axis) becomes $\sqrt{2}u+z_m$ from the results of calculation (see Fig. 2-5). The extraporated range R_e becomes 0.78 R_m and 0.62 R_m for the Makarov's and Wittry's model, respectively.

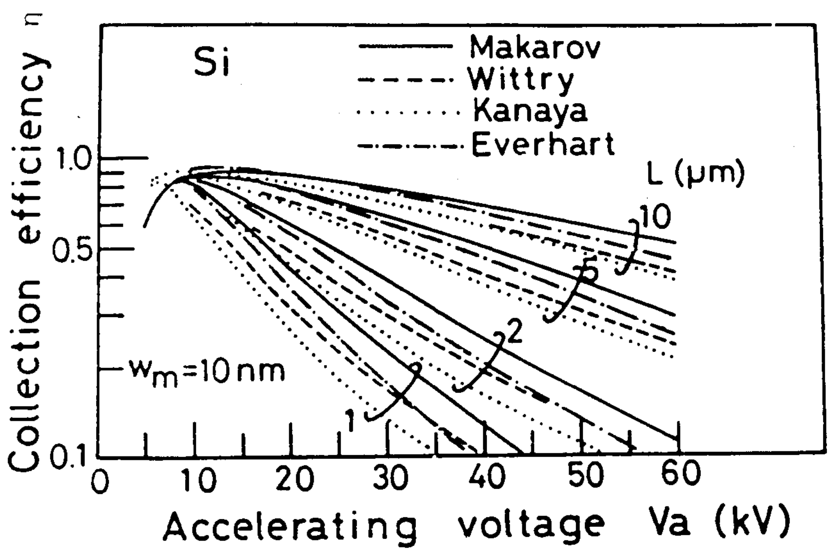

Fig. 2-6 Collection efficiency η vs. V_a curves for Si Schottky diode. The values of L are 10, 5, 2 and 1 μm from upper to lower group of curves,respectively. The results using the Makarov's, Wittry's, Kanaya's and Everhart's models are expressed by the solid, broken,dotted, and dashed and dotted lines, respectively. The values of w_m and w_d are 10 nm and 0.5 μm, respectively.

Figure 2-6 shows the collection efficiency in Si using the four different models of Makarov, Wittry, Kanaya and Everhart by the solid, broken, dotted, and dashed and dotted lines, respectively. The value of L is 10.0, 5.0, 2.0 and 1.0 μm from upper to lower group of curves, respectively. The values of w_m and w_d are taken as typical values of 10 nm and 0.5 μm, respectively. The value of w_m is multiplied by 8.2 in the calculation owing to the difference of densities between Au and Si as discussed before. The value of L larger than 10 μm cannot be determined accurately because EBIC hardly changes even if L varies. The gradient of the curve of the Everhart's model is slightly steeper than those of the Makarov's and Wittry's models which almost agree with each other. And so, the estimated value of L by the Everhart's model becomes larger than that by the Makarov's or Wittry's model for the same η vs. V_a curve (e.g. L=1 μm by the Everhart's model becomes 0.7 μm if the Makarov's model is used). The gradient of the curve of the Kanaya's model is almost equal to that of the Everhart's model, but the absolute value of the former is 30 % smaller than that of the latter for the same value of L. Therefore, the estimated L by Kanaya's model almost agree with that by the Everhart's model, but the value of E_{pc} using the former is 30 % smaller than that using the latter.

As mentioned before, the electron range is inversely proportional to the density of the material. The electron range derived by Everhart in Si can be applied to GaAs considering the difference of the densities between Si and GaAs. The calculated values are plotted by the dashed and dotted line in Fig. 2-3. The ranges of the Makarov's and Wittry's models are larger than that of the Everhart's model. One of the reasons for the disagreement is the different definitions of the electron range, i.e. Makarov and Wittry used the maximum range R_m, but Everhart used the extraporated range R_e. In order to compare these values, the extraporated ranges for the Makarov's and Wittry's models in GaAs are deduced (see footnote in page 23), and become 0.75 R_m and 0.62 R_m, respectively. For example, in the case of V_a=30 kV, the values of R_m for Makarov's and Wittry's models are 3.4 and 4.8 μm, and then the values of R_e become 2.6 and 3.0 μm, respectively. The value of R_e in the Everhart's model (2.9 μm at V_a=30 kV) is slightly larger than that of the Makarov's model, but agrees with that of the Wittry's model.

2-3. Experimental results in GaAs

A conventional SEM was used for the primary electron beam which was modulated at 3 kHz with a chopping coil inserted into the beam path. The induced current was measured from the voltage drop across the load resistance which was connected to the Schottky barrier with an ohmic contact. The signal was detected by a lock-in amplifier. The beam current was measured by a Faraday cage. The beam was somewhat defocussed (Φ=10 μm, Φ: beam diameter) in order to avoid high injection. The induced current was not changed even if the beam was irradiated at the same point for an hour.

The Schottky barrier was made on n-type GaAs (Sn doped, $n=6.2 \times 10^{16}$ cm^{-3}) by evaporating Au of about 10 nm thick in a vacuum of about 10^{-7} Torr. The ohmic contact was obtained by evaporating Au-Ge and alloying at 400 °C for 2 min. The carrier density and the depletion layer width were determined by C-V measurements.

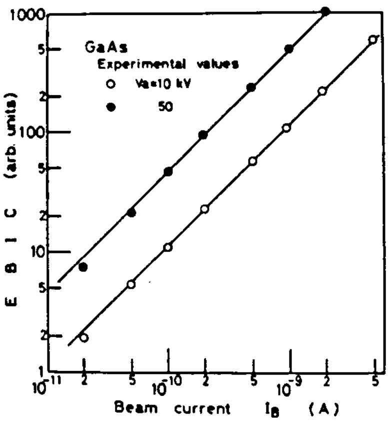

Fig. 2-7

Measured EBIC in GaAs(Sn-doped, $n=6.2\times10^{16}$ cm^{-3})Schottky diode at V_a=10 and 50 kV. The beam current was changed in the range of $2\times10^{-11}\leqq I_B\leqq5\times10^{-9}$ A. The open and solid circles are the experimental results for V_a= 10 and 50 kV, respectively, and the gradients of the solid lines are unity.

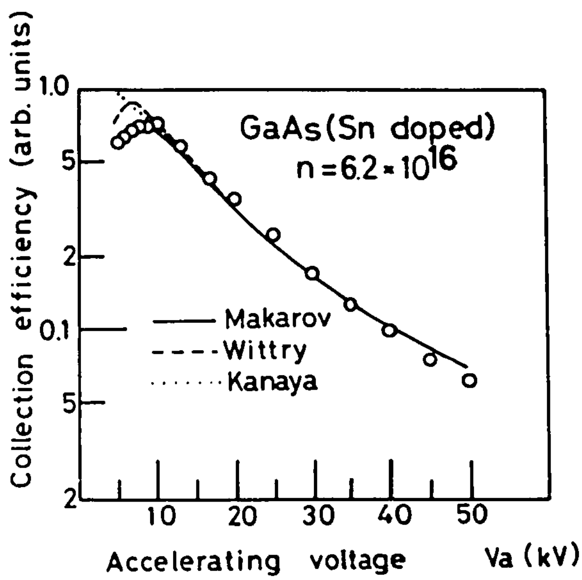

Fig. 2-8

Curve fittings of the experimental results to the theoretical collection efficiencies in GaAs Schottky diode. The solid,broken and dotted lines are the results using the Makarov's, Wittry's and Kanaya's models, respectively. V_a is changed from 5 to 50 kV with the fixed value of $I_B=10^{-10}$ A; w_m=10 nm and w_d=0.15 μm.

	L (μm)	E_{pc} (eV)
Makarov	0.3	4.8
Wittry	0.3	4.1
Kanaya	0.5	4.1

Tab. 2-1 Estimated values of L and E_{pc} in GaAs using the Makarov's,Wittry's and Kanaya's models, respectively.

The value of EBIC at V_a=10 and 50 kV are shown by the solid lines in Fig. 2-7 when the beam current I_B is changed in the range of $2 \times 10^{-11} \leqq I_B \leqq 5 \times 10^{-9}$ A. If the minority carrier concentration exceeds the thermal equilibrium concentration of majority carriers (i.e. high injection), the minority carrier lifetime is prolonged [12]. Therefore, EBIC becomes to increase superlinearly with the number of generated carriers, i.e. with I_B for a fixed value of V_a. In this experiment, EBIC increases linearly with I_B at both V_a's, which shows the low injection. The experimental results are shown by circles in Fig. 2-8 when V_a is changed in the range of $5 \leqq V_a \leqq 50$ kV at the fixed value of $I_B=10^{-10}$ A. Theoretical collection efficiencies using the Makarov's, Wittry's and Kanaya's models are shown by the solid, broken and dotted lines, respectively in Fig. 2-8. The values of L and E_{pc} determined by fitting the experimental data to the theoretical curves are tabulated in Tab. 2-1 for the three different models of Makarov, Wittry and Kanaya. The collection efficiency by the Makarov's model showed fairly good agreement with the experimental results, but that using the Wittry's model is slightly larger than the experimental values in the low V_a region ($V_a \leqq 10$ kV). The discrepancy in the low V_a region becomes large if the Kanaya's model is used. In the case of Wittry's and Kanaya's models, the experimental data were fitted in the range of high V_a ($V_a \geqq 15$ kV). The estimated values of L is 0.3 μm by using both the Makarov's and the Wittry's models, but that using the Kanaya's model is 0.5 μm and about twice of the result by the Makarov's and Wittry's models. The values of E_{pc} determined by the Makarov's, Wittry's and Kanaya's models are 4.8, 4.1 and 4.1 eV, respectively. By the normal incidence method of EBIC, Wu and Wittry [3] and Kobayashi et al. [13] determined E_{pc} as 4.68 and 4.57 eV, respectively, which are almost equal to the result using the Makarov's model, but are about 10 % larger than the value obtained by the Wittry's and Kanaya's models.

2-4. Summary

The values of L and E_{pc} can be determined from the dependence of EBIC on V_a by the normal incidence method. The minority carrier generation distribution plays an important role in the analysis of EBIC. Various generation distribution models are compared with each other uniting the different definitions of the electron range (i.e. maximum range and extraporated range).

In GaAs, Gaussian distributions proposed by Makarov and Wittry have large surface concentrations, and the peaks of the distributions exist at about 0.13 of the maximum electron range. Kanaya's model has evenly spreaded distribution owing to the assumption of the uniform concentration of the generated electron-hole pairs. The value of L larger than 5 μm cannot be determined definitely because EBIC hardly changes even if L varies. The estimated L by the Makarov's model almost agrees with that by the Wittry's model, but E_{pc} determined by the former is 10 ∿ 20 % larger than that by the latter.

In Si, the peaks of the generation distribution become deeper than those in GaAs because the density of Si is about half of that of GaAs. The largest value of L that can be determined definitely becomes twice of that of GaAs because the electron range in Si is about twice of that in GaAs. The estimated L by the Makarov's or Wittry's model is about 30 % smaller than that by the Everhart's model.

In the experiments in GaAs, the estimated L by the Makarov's model agreed with that by the Wittry's model, but the estimated E_{pc} by the former was 4.8 eV and about 17 % larger than that by the latter.

References

[1] W. Czaja: J. Appl. Phys. 37 , 4236 (1966)

[2] J. F. Bresse: " Scanning Electron Microscopy /1972/ part I " (IITRI, Chicago, Ill.) p.105

[3] C. J. Wu and D. B. Wittry: J. Appl. Phys. 49 , 2827 (1978)

[4] K. Kanaya and S. Okayama: J. Phys. D: Appl. Phys. 5 , 43 (1972)

[5] G. E. Possin and C. G. Kirkpatrick: J. Appl. Phys. 50 , 4033 (1979)

[6] T. E. Everhart and P. H. Hoff: J. Appl. Phys. 42 , 5837 (1971)

[7] G. D. Archard: J. Appl. Phys. 32 , 1505 (1961)

[8] D. B. Wittry and D. F. Kyser: J. Appl. Phys. 38, 375 (1967)

[9] T. S. Rao-Sahib and D. B. Wittry: J. Appl. Phys. 40 , 3745 (1969)

[10] V. V. Makarov: Sov. Phys. Semicond. 9 , 722 (1975)

[11] Von A. E. Gruen: Z. Naturforsch. 12a Heft 2, 89 (1957)

[12] J. Cornu, R. Sittig and W. Zimmermann: Solid-State Electron. 17 , 1099 (1974)

[13] T. Kobayashi, T. Sugita, M. Koyama and S. Takayanagi: IEEE Trans. Nucl. Sci. NS-19 , 324 (1972)

III. DETERMINATION OF DIFFUSION LENGTH, SURFACE RECOMBINATION VELOCITY AND ELECTRON-HOLE PAIR CREATION ENERGY BY THE LINE SCAN METHOD

3-1. Introduction

An electron beam induced current (EBIC) method is a convenient technique to measure the minority carrier diffusion length L and the surface recombination velocity s in semi-conducting materials. In the line scan method, L and s can be determined from the dependence of EBIC on the scanning distance when the electron beam is scanned across the barrier. Berz and Kuiken [1] gave a detailed theory for the determination of L and s, and Opdorp [2] investigated experimentally the influence of surface recombination on EBIC. Jastrzebski et al. [3] measured L and s for different generation depths by varying the accelerating voltage of an electron beam.

In those studies, the generation source was assumed to be a point, but in practice the region excited by the electron beam has a finite volume. Chi and Gatos [4] determined the junction depth by an EBIC technique assuming a finite generation volume. Czaja [5] and Bresse [6] measured the physical parameters, such as L and the electron-hole pair creation energy E_{pc}, when the electron beam was directed normal to the barrier plane. Shea et al. [7] investigated the resolution limits of the EBIC line scan method: they obtained a one-dimensional lateral dose function, and applied it to the measurement of L in the Cu_xS:CdS system. However, they did not discuss the effect of surface recombination on EBIC. Since the surface recombination is strongly connected with the depth of generation, a three-

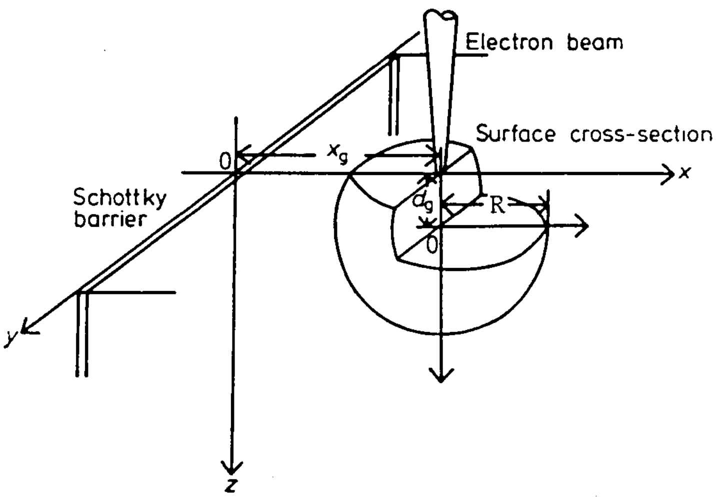

Fig. 3-1 Schematic view of experimental conditions and definitions of the coordinate systems.

dimensional generation distribution must be taken for the detailed analysis of EBIC [8].

In this chapter, firstly, we discuss the surface recombination effect on EBIC assuming a point source, and then, describe the influence of the generation volume on EBIC in the line scan method, taking account of surface recombination. We have studied EBIC theoretically for the finite volume source which is dependent on the accelerating voltage, and show an improved method for the determination of physical parameters of semiconducting materials based on experimental results obtained in Si.

3-2. Surface recombination effect considering point source

For simple theoretical consideration, we take a Schottky diode. As shown in Fig.3-1, the Schottky barrier is in the y-z plane. The electron beam is incident perpendicular to the sample surface, and the scanning direction is along the x-axis which is normal to the barrier plane.

The generation source is considered to be a point at a distance x_g from the barrier, and at a depth d_g from the surface corresponding to the accelerating voltage V_a. The position is $(x_g, 0, d_g)$. The steady state excess minority carrier distribution is obtained from the following diffusion equation.

$$D\nabla^2 p = \frac{p}{\tau} - g\,\delta\,(x-x_g, y, z-d_g), \qquad (3\text{-}1)$$

where D is the diffusion constant, τ is the lifetime and g is the generation rate of electron-hole pairs. When the sample dimensions are assumed to be sufficiently large

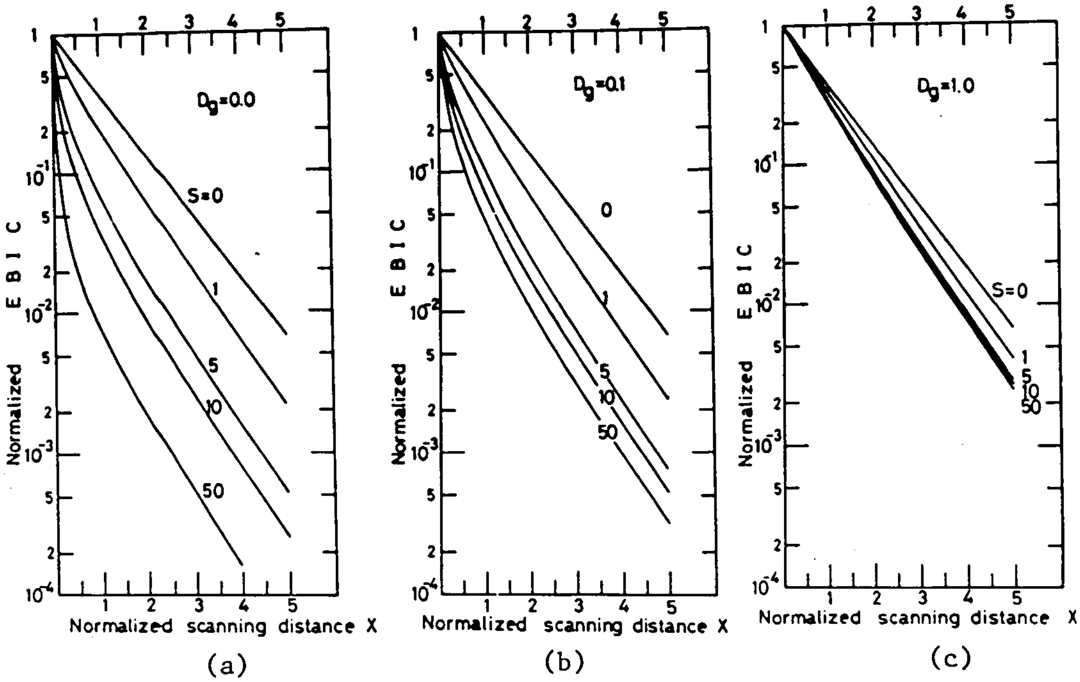

Fig.3-2 Normalized EBIC vs. normalized scanning distance X curves for different values of the surface recombination velocity parameter (see text) S. Normalized generation depth D_g is 0.0, 0.1 and 1.0 in (a), (b) and (c), respectively.

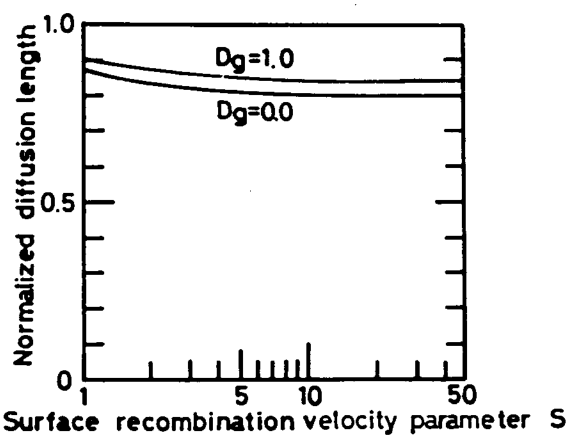

Fig. 3-3 Estimated diffusion length L* directly from the slopes of the curves between the points at X=2 and 3; S varies from one to 50.

compared with the diffusion length, the boundary conditions are

$$D \left.\frac{\partial p}{\partial z}\right|_{z=0} = s \left. p \right|_{z=0} \quad \text{(at the surface)}, \tag{3-2a}$$

$$\left. p \right|_{x=0} = 0 \quad \text{(at the Schottky barrier)}, \tag{3-2b}$$

$$\left. p \right|_{x=+\infty} = 0 \quad . \tag{3-2c}$$

Once the distribution p is known, the EBIC can be found as follows.

$$j = e\, D \int_0^{+\infty} \int_{-\infty}^{+\infty} \left.\frac{\partial p}{\partial x}\right|_{x=0} dy\, dz \ , \tag{3-3}$$

where e is the charge of an electron. The value of j was calculated using a image source-and-sink distribution [1,2]. When the dimensionless variables are used, j becomes as follows.

$$J = \frac{j}{e\, g} = \frac{2}{\pi} X_g \Big\{ \int_0^{D_g} \frac{K_1(\sqrt{X_g^2+T^2})}{\sqrt{X_g^2+T^2}}\, dT + \int_{D_g}^{+\infty} \exp(-S(T-D_g)) \frac{K_1(\sqrt{X_g^2+T^2})}{\sqrt{X_g^2+T^2}}\, dT \Big\} \ , \tag{3-4}$$

where $X_g=x_g/L$, $D_g=d_g/L$, $S=s/(L/\tau)$ and T is the variable for integration. The function $K_1(\sqrt{X_g^2+T^2})$ is the second-modified first-order Bessel function. The EBIC is normalized to be unity when all the generated carriers contribute to EBIC.

In Figs. 3-2 (a), (b) and (c), the logarithm of J is plotted vs. $X (\equiv x/L)$ based on eq.(3-4) over the range of $0 \leqq X \leqq 5$ for $S=0 \sim 50$. The value of D_g is 0.0, 0.1 and 1.0 in (a), (b) and (c), respectively. For S=0, the integral in eq.(3-4) leads to $J=\exp(-X)$ which yields straight lines as shown in Fig. 3-2 . On the other hand, all curves for $S > 0$ deviate from the straight line. The surface recombination gives much effect on the excess carrier distribution as the generation depth becomes shallower. When D_g is 0.0 and 0.1, the values of logJ decrease superlinearly over the interval of $0 \leqq X \leqq 2$, and almost linearly over the range of $X \geqq 2$. When D_g is 1.0, the surface recombination has a slight influence, and the values of logJ decrease almost linearly over the interval of $0 \leqq X \leqq 5$. However, the slopes show substantial deviation from unity. The estimated values of diffusion length directly from the slopes of the curves in the linearly decreasing region $2 \leqq X \leqq 3$ are put as L* and plotted against S in Fig.3-3 for $D_g = 0.0$ and 1.0. In ordinary semiconductors, S varies from 1 to 50. Over this range, L* is about 80 to 90 % of the real value L.

When we evaluate the accurate values of L and S, we must fit the experimental data to the theoretical curves over the whole range of $0 \leqq X \leqq 5$. We can estimate S by fitting particularly over the interval of $0 \leqq X \leqq 2$, because the effect of the surface recombination appears remarkably in this interval.

3-3. Analysis of electron beam induced current taking three-dimensional generation distribution into account

In §3-2, the minority carrier distribution is assumed to be a point. But, in practice, the generation distribution has a finite volume in connection with V_a. The generation distribution must be taken into account when the extent of the generation distribution cannot be ignored compared with L.

Electron penetration into solid materials has been studied by many authors. The minority carrier generation distribution along the depth was discussed in detail in Chapter II . Wittry and Kyser [9] assumed the depth dose function to be a Gaussian distribution, and obtained good agreement with experiments. Everhart and Hoff [10] assumed a polynomial function to explain their experimental results in the $Al-SiO_2-Si$ system. In those studies only the distribution along the z axis was discussed, so the distribution along the x axis was not considered. Shea et al. [7] defined the lateral dose function along the x axis from Von Grün's [11] data, but did not discuss the influence of surface recombination in detail. Since the influence of surface recombination on EBIC depends on the depth from the surface, we must take the distribution of generated minority carriers in the x-z plane. We use the modified diffusion model of Kanaya and Okayama [12] . The model is very simple, but is sufficient for the first-order approximation to the three-dimensional generation distribution. According to the model, the electrons penetrate straight into the material to the maximum energy dissipation depth, and then scatter equally in all directions, making electron-hole pairs. The shape of the generation region becomes a sphere, part of which is above the surface.

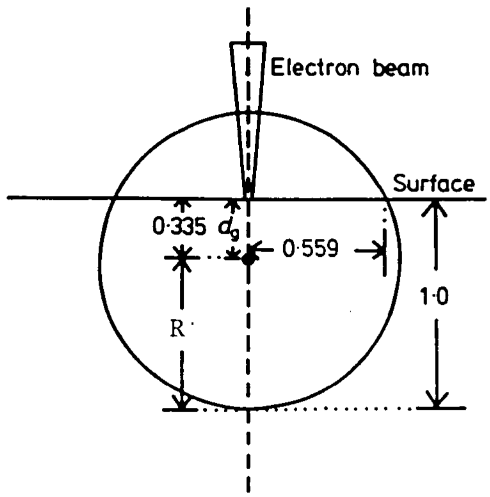

Fig. 3-4 Schematic view of electron penetration; d_g is the maximum energy dissipation depth.

V_a (kV)	d_g (μm)	R (μm)
10	0.47	1.00
20	1.49	2.95
30	2.91	5.74
40	4.65	9.20
50	6.69	13.2

Tab. 3-1 Values of the center d_g of the generation volume and the radius R in Si for several values of accelerating voltage V_a.

The center d_g of the sphere (i.e. the maximum energy dissipation depth) and the radius R are dependent on the accelerating voltage V_a, but the ratio d_g/R is assumed to be a constant, as shown in Fig. 3-4, even when V_a is varied. The values of d_g and R in Si for several values of V_a are given in Tab.3-1, calculated with the aid of the equations of Kanaya and Okayama [12].

We divide the semi-sphere into many segments of length less than L, and represent each segment by one point source. The density of the electron-hole pairs is assumed to be uniform within the sphere to simplify the analysis. Then, the generation strength g of each point source is given by the following relation:

$$\Sigma g = G \quad , \tag{3-5}$$

where G is the whole generation strength, and Σ expresses the total summation within the semi-sphere under the sample surface.

The EBIC for the finite volume source is derived by summimg up the solution of the diffusion equation for each point source, which is expressed by eq.(3-4). When the distance between the barrier and the irradiated point x_g becomes smaller than R, some of the point sources are forced out of the diode, and cannot contribute to EBIC. Thus the EBIC decreases near the barrier plane. We call this phenomenon an edge effect. To simplfy the calculation, we assume that the EBIC contributed by the forced-out sources is zero. This edge effect must be taken into account when the generation volume is large in comparison with the diffusion length. We show an example for L=8 μm and S=20. When V_a is 10 kV, the radius R is small compared with L, and the generation source can be assumed as a point. The logarithm

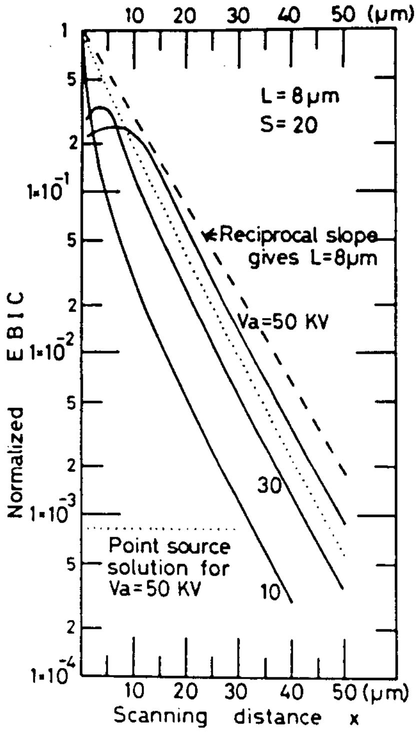

Fig. 3-5 Normalized EBIC versus scanning distance x for the finite volume source. The diffusion length L is 8 μm, and the surface recombination velocity parameter S (see text) is 20. The accelerating voltage V_a is 50, 30 and 10 kV from upper to lower solid curve, respectively. The dotted curve is the point source solution for V_a=50 kV, and the dashed line is the gradient,the reciprocal of which gives L=8 μm.

of EBIC, J, is plotted with a full curve as a function of the scanning distance x in Fig. 3-5: logJ decreases superlinearly over the interval $0 \leqq x \leqq 2L$ (i.e. 16 μm in this case), and decreases almost linearly over the range $x \geqq 2L$. The slope in the range $0 \leqq x \leqq 2L$ is influenced very much by surface recombination. One can estimate s by fitting the experimental data to the theoretical curve in this range. When V_a is 30 or 50 kV, the radius R becomes of the same order as L, and the generation volume cannot be assumed as a point. Then, we divide the semi-sphere into many segments of 1 μm^3. The calculated values of EBIC using the finite volume source method are shown in Fig. 3-5. The logJ vs. x curves show a maximum near the barrier plane (x=4 and 7 μm at V_a=30 and 50 kV, respectively), and logJ decreases almost linearly beyond these maximum points. The maximum value of J becomes small as V_a increases. The surface recombination does not affect the shape of the curves, and so L can be determined mainly from the slope of the linear region of these curves independently of s. The reciprocal slope of this linear portion gives 7 μm, which is 87 % of the real diffusion length.

The value of E_{pc}, by which an electron-hole pair is created, can be determined from the absolute value of EBIC [13]. The value of J in the case of S=50 is about 70 % of that in the case of S=1 when V_a is 50 kV, and so we make large errors in the determination of E_{pc} if we do not consider the surface recombination effect.

The point source solution at V_a=50 kV is shown in Fig. 3-5 by the dotted line, when the generation occurs at the maximum energy dissipation depth (i.e. 6.7 μm from Tab. 3-1).
The slope of the point source solution over the range $x \geqq 2L$ is almost equal to that of the volume source solution, but the normalized EBIC is 60 % of that of the volume source solution.

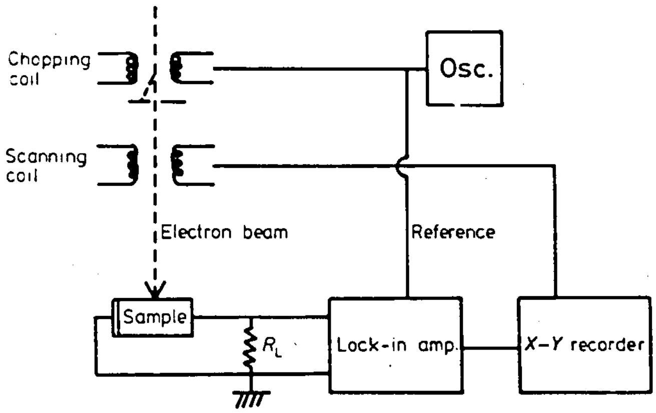

Fig. 3-6 Schematic diagram of the experimental set-up.

3-4. Experimental results in Si

A schematic diagram of the experimental set-up is shown in Fig. 3-6. The accelerating voltage is varied from 10 to 50 kV. The primary electron beam current is measured by a Faraday cage, and about 2×10^{-10} A. The induced current was measured from the voltage drop across the load resistance R_L . The current I_L which flows through the resistance is expressed as follows.

$$I_L = I_{SC} - I_o\{\exp[(e/kT)I_L R_L]-1\}, \qquad (3-6)$$

where I_0 is the backward saturation current, and I_{SC} is the short-circuit current, which is the real EBIC. In order to neglect the second term of eq.(3-6), the EBIC was measured in the following condition

$$I_L R_L \ll kT/e \quad . \qquad (3-7)$$

In the present experiment, the EBIC was measured at room temperature, and so, $I_L R_L$ was kept less than 1 mV.

The electron beam was chopped at 3 kHz with a chopping coil inserted into the beam path. Signals as small as 1 μV could be measured with a good signal to noise ratio using a lock-in amplifier.

The samples were n-type Si with resistivity ρ of 1.0 and 0.1 Ω cm. Ohmic contacts were made by evaporating antimony-doped gold on to the sample, and alloying at 400 °C for 2 min. Schottky contacts were made by evaporating gold in a vacuum as low as 10^{-7} Torr. The sample was inserted into a vacuum chamber for EBIC measurement immediately after it was cleaved and measured

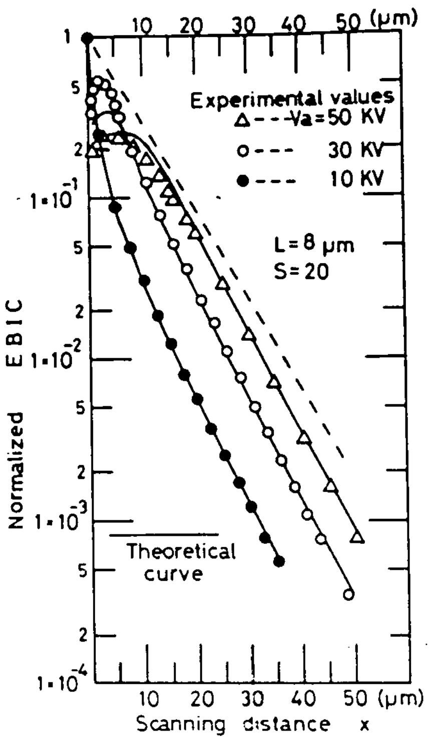

Fig. 3-7

Experimental results for sample A (ρ=1 Ωcm) where L= 8 μm and S=20. Full curves are the theoretical ones.

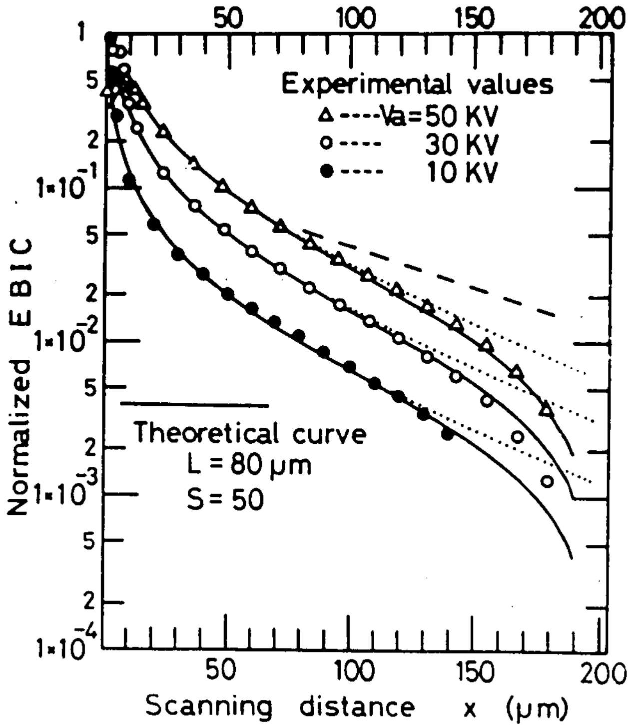

Fig. 3-8

Experimental results for sample B (ρ=0.1 Ωcm) where L=80 μm and S=50. Full curves are the theoretical ones. Values without the influence of an ohmic contact are shown by dotted curves.

in a vacuum as low as 1×10^{-8} Torr. The residual gases on the cleaved surface were cleaned by argon ion sputtering to avoid contamination of the surface by an irradiated electron beam.

The experimental results of sample A (ρ=1.0 Ω cm) are shown in Fig. 3-7 for V_a = 10, 30 and 50 kV, respectively. Each full curve is the theoretical one for the case of L=8 μm and S=20. If the diffusion constant D is taken as 16 cm^2s^{-1} , the lifetime τ is 4×10^{-2} μs, and the surface recombination velocity s is 4×10^5 cm s^{-1}. Surface recombination has a greater effect as the generation depth becomes shallower, that is, V_a becomes lower. And so, the values of S and L can be estimated mainly from the curves for the lowest and the highest V_a (i.e. 10 and 50 kV in this experiment), respectively. The experimental results for each accelerating voltage agree very well with the theory. The experimental curves for V_a = 10, 30 and 50 kV have a maximum at x=0, 2 and 4 μm, respectively, and each maximum value becomes smaller as V_a increases, as described in the theory. However, the maximum value and the position where the EBIC shows a peak deviate slightly from the theory in the cases of V_a= 30 and 50kV. This discrepancy may be attributed to the assumption of uniform density of generation. The actual distribution may be localized at the center of the generation volume [9], and more detailed treatment for the generation shape and the generation density is needed.

In the case of the localized distribution of generation, we can apply the same method as discussed in §3-3. If the constant g is changed into an appropriate variable which expresses the localized distribution, better results will be obtained. However, the assumption of the uniform density is sufficient for the qualitative analysis of the influence of the generation volume on EBIC.

The experimental results of sample B (ρ=0.1 Ω cm) are indicated in Fig. 3-8 in the same way as sample A. The values of L and S are 80 μm and 50, respectively. If D is 16 cm^2s^{-1}, τ is 4 μs and s is 1×10^5 cm s^{-1}. In this case, L is greater than the generation volume even when V_a=50 kV, and the volume source effect appears less clearly than in sample A. The discrepancy within the interval $0 \leqq x \leqq 15$ μm is due to the same reason as that discussed in the case of sample A. The slopes of the curves over the range $15 \leqq x \leqq 100$ μm are less steep as V_a becomes higher, because the influence of surface recombination decreases. The influence of ohmic contact appears over the range $x \geqq 120$ μm, since the diffusion length is about half of the sample thickness of 200 μm. Theoretical values calculated using the mirror image method [14] discussed in Chapter V are shown by full curves in Fig. 3-8. Values without the influence of an ohmic contact are also shown by dotted curves.

The scanning surface was not affected by an electron beam of the order of 2×10^{-10} A, because the same result was obtained for shallow excitation (V_a=10 kV) after the sample was irradiated for 1 h at V_a= 10 ∿ 50 kV.

The depletion layer width is not brought into consideration because of its narrowness compared with the scanning distance. The electron beam diameter of about 50 nm in this experiment is not taken into account, since it is very small in comparison with the generation region even if V_a is 10 kV.

If the beam current is kept constant, the generation density decreases with increasing V_a, because the generation volume increases superlinearly with V_a. When the beam current is 2×10^{-10} A, and V_a is 10 kV, the excess minority carrier density at the generation point is about 5×10^{14} cm^{-3}(the maximum generation density in this experiment), following the discussion in ref. [1], which is smaller than the majority carrier density in the samples. Therefore, the value of L is measured at the low injection level.

3-5. Summary

The generation volume of minority carriers has a considerable effect on the EBIC line scan profiles, especially when it is equal to or larger than the diffusion length. We investigated the dependence of EBIC on x for general surface recombination velocity in the case of the finite volume source.

When V_a is low, and the generation depth is shallow, surface recombination has a large effect on EBIC. When V_a is high, and the generation depth is as large as the diffusion length, the generation region can no longer be assumed as a point, and the finite volume source should be used in the analysis. The theoretical calculation shows that surface recombination has only a slight effect on the shape of logJ vs. x curves, but affects the absolute value of J. The accurate values of L, s and E_{pc} should be estimated by fitting the experimental data to the theoretical curves for all accelerating voltages. Experimental results in the measurement of L and s on Si Schottky diodes showed good agreement with the theory at both low and high V_a.

The experimental result that EBIC has a maximum near the barrier plane was explained qualitatively using the simple model of the finite volume source. It could not be explained by the point source solution. Further investigation of this edge effect will clarify the generation distribution by an electron beam.

References

[1] F. Berz and H. K. Kuiken: Solid-State Electron. 19 , 437 (1976)

[2] C. van Opdorp: Philips Res. Rep. 32 , 192 (1977)

[3] L. Jastrzebski, J. Lagowski and H. C. Gatos: Appl. Phys. Lett. 27 , 537 (1975)
J. Appl. Phys. 48 , 1730 (1977)

[4] J. Y. Chi and H. C. Gatos: IEEE Trans. Electron. Dev. ED-24 , 1366 (1977)

[5] W. Czaja: J. Appl. Phys. 37 , 4236 (1966)

[6] J. F. Bresse: "Scanning Electron Microscopy /1972/ Part I " (SEM Inc. IITRI Chicago) pp.105-112

[7] S. P. Shea, L. D. Partain and P. J. Warter: "Scanning Electron Microscopy /1978/ Vol.I " (SEM Inc. AMF O'Hare) pp.435-444

[8] G. V. Spivak, G. V. Saparin and L. F. Komolova: "Scanning Electron Microscopy /1977/ " (SEM Inc. IITRI Chicago) pp.191-199

[9] D. B. Wittry and D. F. Kyser: J. Appl. Phys. 38 ,375 (1967)

[10] T. E. Everhart and P. H. Hoff: J. Appl. Phys. 42 ,5837 (1971)

[11] A. E. von Grün: Z. Naturforsch. 12a , 89 (1957)

[12] K. Kanaya and S. Okayama: J. Phys. D: Appl. Phys. 5 , 43 (1972)

[13] C. J. Wu and D. B. Wittry: J. Appl. Phys. 49 , 2827 (1978)

[14] O. von Roos: Solid-State Electron. 21 , 1063 (1978)

IV. ANALYSIS OF THREE-DIMENSIONAL GENERATION DISTRIBUTION BY THE COMBINATION OF THE NORMAL INCIDENCE AND THE LINE SCAN METHODS

4-1. Introduction

The minority carrier diffusion length L and the surface recombination velocity s can be determined by an EBIC technique with both the normal incidence and the line scan methods using SEM as discussed in Chapters II and III. The minority carrier generation distribution by an electron beam plays an important role in the analysis of EBIC. When the dimension of the generation region is comparable with or larger than L, the generation region cannot be assumed as a point, and the generation distribution must be taken into account.

The generation distribution by an electron beam has been investigated by several authors theoretically [1] and experimentally [2-5] . As regards the one-dimensional distribution, a Gaussian [2-3] or polynomial [4] function was assumed for the depth dose function, and the combination of exponential decay functions [5] was used for the lateral dose function. In Chapter III, the influence of the three-dimensional generation distribution on EBIC in the line scan methods was studied, assuming a simple distribution (semisphere) with uniform minority carrier density. In each of these experiments only one method, either line scan or nomal incidence, was taken. The electron penetration depth and the generation distribution differed from each other.

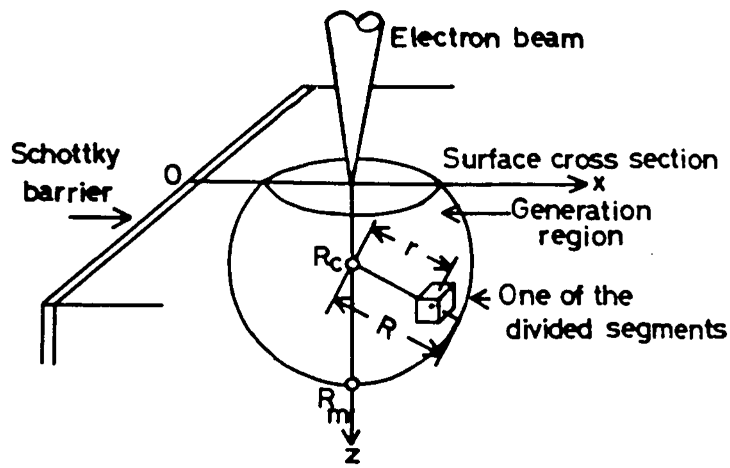

Fig. 4-1 Schematic view of experimental conditions and the definition of the coordinate system.

In this chapter, we measured EBIC by both the line scan and the normal incidence methods in the same sample, and clarified the generation distribution. The influence of the three-dimensional generation distribution on EBIC is discussed assuming that the electron-hole pairs are localized at the center of the generation region. The experimental results for GaAs Schottky diodes are also shown.

4-2. Influence of three-dimensional generation distribution on electron beam induced current

We used a Schottky diode since it can be applied for both the line scan and the normal incidence methods. In the line scan method, the EBIC is calculated taking the generation distribution into account by a similar method discussed in Chapter III. The generation region is divided into many segments the size of which is smaller than L, and each segment is represented by one point source. The EBIC for the finite volume source is derived by summing up the solution of the diffusion equation for each point source.

The distribution is assumed to be spherically symmetric as is shown in Fig. 4-1. The electron-hole pairs generated by an electron beam are considered to be localized at the center R_c of the generation region. The generation strength g along any radius vector from R_c is assumed to be given by

$$g \propto \exp[-C(r^2/R^2)] \quad , \qquad (4\text{-}1)$$

where R is the distance between R_c and the maximum electron range R_m, and r is the distance between R_c and each divided segment (see Fig. 4-1).

The exponent C relates to the distribution density. The density becomes uniform as discussed in Chapter III when C is zero, and the electron-hole pairs localize near R_c when C becomes large. The distribution is assumed in order that the depth dose function may become Gaussian as is reported in the references [2,3].

The value of L should be small in order that it can be measured by both the line scan and the normal incidence methods. Therefore we take GaAs as an example. In the line scan method, we calculate the EBIC intensity (which is called the collection efficiency η, and is normalized to be unity when all the generated carriers contribute to EBIC) for several values of C and R_c/R_m. The value of R_m is given [2] by

$$R_m = 0.0148\ V_a^{\ 1.7} \quad \mu m \quad , \tag{4-2}$$

where V_a is the accelerating voltage in kV. The values of C and R_c/R_m are assumed to be constant even if V_a is varied. When V_a is 10 and 30 kV, R_m becomes 0.74 and 4.8 μm, respectively. We take the typical value of L as 1 μm in order to examine the influence of the generation distribution on EBIC, because the value of R_m is smaller than L at V_a= 10 kV, but larger than L at V_a=30 kV. Since the surface recombination velocity s of GaAs is of the order of 10^5 - 10^6 cm s^{-1} [6-9] , we take values of 1 and 50 as the surface recombination velocity parameter S defined by $S \equiv s/(L/\tau)$ (τ is the lifetime of order of ns).

The results of the calculation are shown in Fig. 4-2. The full curves and the broken curves are for C=8.2, R_c/R_m=0.13 and C=5.4, R_c/R_m=0.13, respectively. These values of C and R_c/R_m are the typical values obtained by the normal incidence method in GaAs [2,3]. The point source solutions (which are obtained by assuming that all the generation occurs at R_c) are also shown by

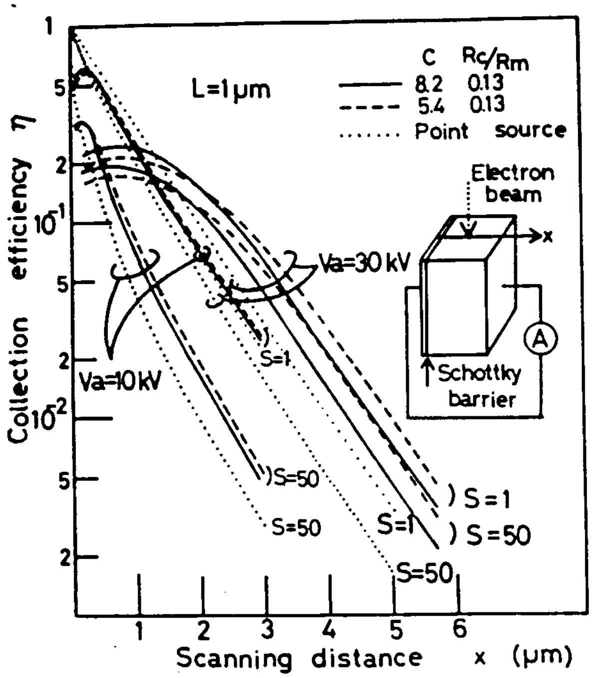

Fig. 4-2 Theoretical collection efficiency η versus scanning distance x curves in the case of the localized generation distribution of minority carriers. The diffusion length L is 1 μm, the surface recombination velocity parameter S (see text) is 1 and 50, and the accelerating voltage V_a is 10 and 30 kV. The full and broken curves are for C=8.2, R_c/R_m=0.13 and C=5.4,R_c/R_m= 0.13, respectively. The dotted curves are the point source solutions.

dotted curves. At V_a=10 kV, the size of the divided segment is taken as 0.05 μm which is smaller than L so that each divided segment can be represented by one point source. In the region $0.5 \leqq x \leqq 1.5$ μm, the logarithm of EBIC decreases superlinearly, and it decreases almost linearly over the range of $x \geqq 1.5$ μm. The tendency appears more apparent as S becomes large. The change of the exponent C makes little difference to the profiles of the curves. The absolute value of η over the range of $x \geqq 0.5$ μm is almost equal to the point source solution when S is 1, but becomes twice that when S is 50. The peaks near the barrier are due to the edge effect as described in Chapter III. At V_a=30 kV, the size of the divided segment is taken as 0.2 μm for the same reason as with V_a=10 kV. The curves are quite different from the point source solution both at S=1 and S=50, because the dimensions of the generation region are large in comparison with L, and the point source assumption is no longer valid in this case. The profiles of the curves reflect the generation distribution as one sees that the profile changes if C varies from 5.4 to 8.2. When S is varied from 1 to 50, the profile does not change at the same C value, but η decreases by about 30 % of that of S=1. It should be noted that the surface recombination has an influence on the absolute value of EBIC even if the value of R_m (4.8 μm at V_a=30 kV) is much greater than L. Therefore, we can evaluate L mainly from the slope of the linear region at low V_a considering the surface recombination effect, and estimate the generation distribution from the profiles of the curves in the case of high V_a.

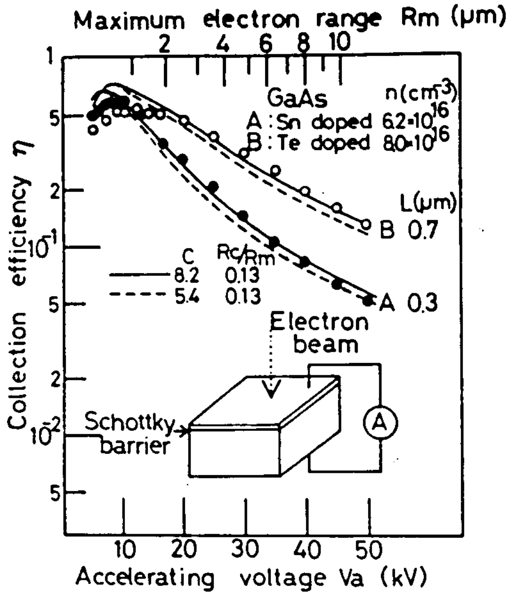

Fig. 4-3 Experimental results of the normal incidence method for the sample A (Sn doped GaAs, $n=6.2\times10^{16}$ cm^{-3}, L=0.3 μm)and the sample B (Te doped GaAs, $n=8.0\times10^{16}$ cm^{-3}, L=0.7 μm). Experimental values are shown by circles. The full and broken curves are theoretical curves for C=8.2, $R_c/R_m=0.13$ and C=5.4, $R_c/R_m=0.13$, respectively;$w_m=10$ nm and $w_d=0.15$ μm.

The electron-hole pair creation energy E_{pc} is obtained from the following equation [10]:

$$\eta = E_{pc} \frac{I_{EBIC}}{I_B V_a k} \quad , \qquad (4\text{-}3)$$

where I_B is the beam current, and k is the correction factor for the back-scattered electrons. As described previously, the value of η is influenced by S even when V_a is high, and so we must take the surface recombination effect into account when we evaluate E_{pc}.

4-3. Three-dimensional generation distribution in GaAs

The same apparatus and the lock-in technique were used as described in §3-4. The Schottky barrier was made on n-type GaAs wafers by evaporating Au of about 10 nm thick in a vacuum of about 10^{-7} Torr. The ohmic contact was obtained by evaporating Au-Ge and alloying at 400 °C for 2 min. The carrier density n of each sample was determined by C-V measurements.

The experimental results of the normal incidence method for the sample A (Sn doped, $n=6.2 \times 10^{16}$ cm^{-3}) and the sample B (Te doped, $n=8.0 \times 10^{16}$ cm^{-3}) are shown in Fig. 4-3 by full and open circles, respectively. The value of V_a was varied between 5 and 50 kV. The EBIC intensity increased linearly with I_B within the range of $1 \times 10^{-11} \leqq I_B \leqq 1 \times 10^{-9}$ A when V_a was fixed, which satisfied the low injection level condition. The collection efficiency η was calculated by the same method reported in ref.[10], by changing R_c/R_m from 0.1 to 0.25 and C from 3.0 to 9.0, respectively. The best fit curves with the experimental results were obtained in the case of L=0.3 and 0.7 μm for samples A and B, respectively, when R_c/R_m=0.13 and C=8.2 were used. The values of

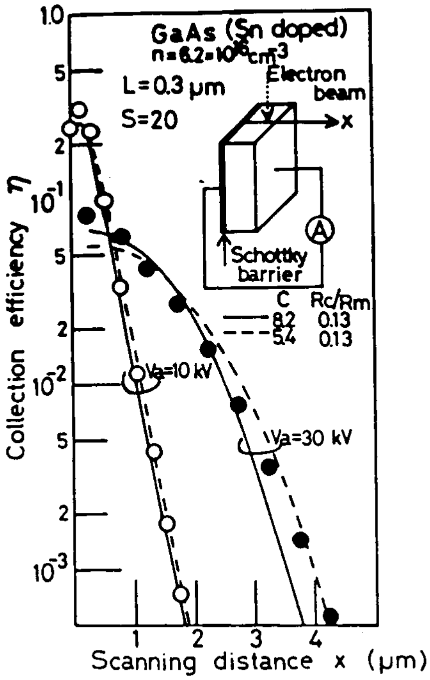

Fig. 4-4

Experimental results of the line scan method for the sample A (Sn doped GaAs, $n=6.2\times10^{16}$ cm^{-3}). The full and broken curves are theoretical curves for C=8.2, R_c/R_m =0.13 and C=5.4, R_c/R_m=0.13, respectively;L=0.3 μm, S=20.

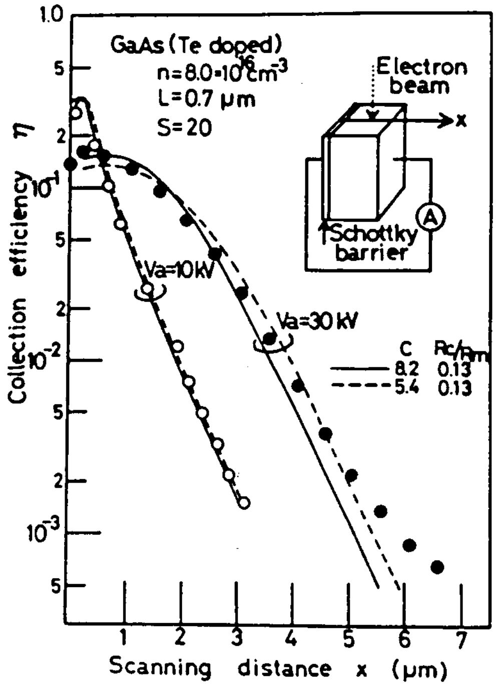

Fig. 4-5

Experimental results of the line scan method for the sample B (Te doped GaAs, $n=8.0\times10^{16}$ cm^{-3}). The full and broken lines are theoretical curves for C=8.2, R_c/R_m =0.13 and C=5.4, R_c/R_m=0.13, respectively;L=0.7 μm, S=20.

R_c/R_m and C agrees with the reported values [2]. The full and broken curves in the figure are theoretical curves for C=8.2, R_c/R_m=0.13 and C=5.4, R_c/R_m=0.13, respectively. The discrepancy between the theoretical curves and the experimental values at low V_a can be explained in the following way. The generation region becomes shallow near the surface at low V_a, and the EBIC is mainly contributed by the seperated electron-hole pairs in the space-charge region just under the surface. In the theoretical calculation, it is assumed that there is no recombination in the space-charge region. But, in actual fact, the carriers recombine through the various traps, which reduces the EBIC.

The experimental results of the line scan method for the samples A and B are shown by circles in Figs. 4-4 and 4-5, respectively. The theoretical curves are expressed by the full (C=8.2, R_c/R_m=0.13) and the broken (C=5.4, R_c/R_m=0.13) curves in both figures. The EBIC intensity increased linearly with I_B within the range $1 \times 10^{-11} \leqq I_B \leqq 1 \times 10^{-9}$ A when V_a was fixed at 10 or 30 kV, which satisfied the low injection level condition as in the normal incidence method. The theoretical curves calculated using the same parameter determined by the normal incidence method show good agreement with the experimental results at both V_a=10 and 30 kV. When we take into account that the experimental results at V_a=30 kV reflect the generation distribution, the assumed generation distribution by eq.(4-1) with C=5.4∿8.2 and R_c/R_m=0.13 is considered to be appropriate for the three-dimensional generation distribution in GaAs.

The value of k changes from 0.78 to 0.75 when V_a varies from 5 to 50 kV [10]. When we take the appropriate value of k for the measured V_a, E_{pc} can be determined by eq.(4-3). The values of

		Normal incidence	Line scan	
V_a (kV)		5 - 50	10	30
E_{pc} (eV)	GaAs(Sn doped)	4.1	4.4	3.9
	GaAs(Te doped)	3.9	3.9	3.8

Tab. 4-1 Values of the electron-hole pair creation energy E_{pc} in GaAs determined by the normal incidence and line scan methods.

E_{pc} obtained by the normal incidence and the line scan methods are 3.9 ∿ 4.1 eV and 3.8 ∿ 4.4 eV, respectively, as tabulated in Tab. 4-1. By the normal incidence method, Wu and Wittry [10] determined E_{pc} as 4.68 eV, which was about 15 % larger than our results. One reason for the discrepancy is the difference of the generation distributions. The modified Gaussian distribution used by them slightly differed from the Gaussian distribution used in our analysis. Another reason is the accuracy of metal thickness. We estimate the thickness from the weight of the charged Au which is evaporated to make the Schottky barrier. Therefore, the obtained value may be different from the real thickness. In the line scan method, EBIC becomes insensitive to the metal thickness and the traps in the space-charge region, but is influenced by surface recombination as discussed before. Alferov et al. [11] and Wittry and Kyser [12] reported E_{pc} as 3.2 ∿ 4.4 eV and 4.6 eV, respectively, from the peak value of EBIC when the electron beam crossed the p-n junction. Our results of 3.8 ∿ 4.4 eV are in the middle range of their values. In their analyses, they did not take the surface recombination effect into account, and so our results are considered to be more reliable than theirs.

4-4. Summary

The three-dimensional generation distribution by an electron beam in GaAs was investigated by measuring EBIC with a combination of normal incidence and line scan methods.

The profile of the EBIC curves in the line scan method expresses the generation distribution, when V_a is high and the dimension of the generation region is larger than L. The surface recombination does not affect the profile of EBIC, but lowers the collection efficiency. The accurate value of the electron-hole pair creation energy must be determined by taking the surface recombination effect into account.

The experimental results in GaAs Schottky diodes with different diffusion lengths showed that the center of the generation region (i.e. the maximum energy dissipation depth) was located at the point of 0.13 of the maximum electron range, and the radial distribution from the center was shown to be Gaussian with an exponent of 5.4 ∿ 8.2. The electron-hole pair creation energy in GaAs was determined as 3.8 ∿ 4.4 eV.

References

[1] K. Kanaya and S. Okayama: J. Phys. D: Appl. Phys. 5, 43 (1972)

[2] D. B. Wittry and D. F. Kyser: J. Appl. Phys. 38, 375 (1967)

[3] V. V. Makarov: Sov. Phys.-Semicond. 9, 722 (1975)

[4] T. E. Everhart and P. H. Hoff: J. Appl. Phys. 42, 5837 (1971)

[5] S. P. Shea, L. D. Partain and P. J. Warter: "Scanning Electron Microscopy /1978/ Vol.I " (SEM Inc. AMF O'Hare) pp.435-444

[6] L. Jastrzebski, H. C. Gatos and J. Lagowski: J. Appl. Phys. 48, 1730 (1977)

[7] L. Jastrzebski, J. Lagowski and H. C. Gatos: Appl. Phys. Lett. 27 , 537 (1975)

[8] M. Ettenberg, H. Kressel and S. L. Gilbert: J. Appl. Phys. 44 , 827 (1973)

[9] C. A. Hoffman, K. Jarasiunas, H. J. Gerritsen and A. V. Nurmikko: Appl. Phys. Lett. 33 , 536 (1978)

[10] C. J. Wu and D. B. Wittry: J. Appl. Phys. 49 , 2827 (1978)

[11] Zh. I. Alferov, V. M. Andreev, V. I. Korol'kov and V. I. Stremin: Sov. Phys. -Semicond. 4 , 1113 (1971)

[12] D. B. Wittry and D. F. Kyser: J. Appl. Phys. 36 , 1387 (1965)

V. ANALYSIS OF ELECTRON BEAM INDUCED CURRENT CONSIDERING SAMPLE DIMENSIONS

5-1. Introduction

An electron beam induced current (EBIC) method using a scanning electron microscope (SEM) is a convenient technique to measure the minority carrier diffusion length L and the surface recombination velocity s in semiconductors. There have been many theoretical and experimental studies on the line scan method of EBIC. In Chapters III and IV, the EBIC was analyzed quantitatively taking the three-dimensional generation distribution into account by the dividing method, and the improved method to characterize L and s was suggested. When the sample dimensions are less than one or two diffusion lengths, the minority carrier distribution is affected very much by sample dimensions. Roos [1] analyzed EBIC theoretically in the case of thin layers. He calculated the dependence of EBIC on the scanning distance x in the range of $x/L \ll 1$ in the samples with $w/L=1$ and 0.5 (w: layer thickness), and showed that L could not be determined definitely from the slope of the logarithm of EBIC vs. x curve.

In this chapter, to analyze EBIC considering the sample dimensions, we discuss a simple method using an image source-and-sink distribution. We show the dependence of EBIC on x over a full scan range when the length between a potential barrier and an ohmic contact is equal to and smaller than the diffusion length, and mention some important points to be noticed in the determination of L and s. The experimental results in Si Schottky diodes are also shown.

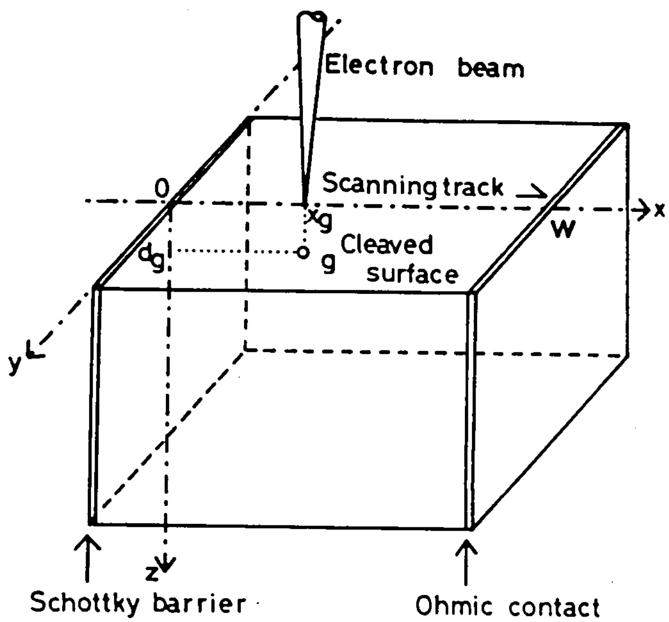

Fig. 5-1 Schematic view of experimental conditions, and definition of the coordinate system.

5-2. Determination of diffusion length and surface recombination velocity

For simple theoretical consideration, we take a Schottky barrier diode. As shown in Fig. 5-1, the Schottky barrier is in the y-z plane, and the electron beam is incident perpendicular to the sample surface (x-y plane). The scanning direction is along the x-axis which is normal to the barrier plane. The generation source is considered to be a point, and is located at $(x_g, 0, d_g)$. The steady state excess minority carrier distribution p is obtained from the following diffusion equation.

$$D \nabla^2 p = \frac{p}{\tau} - g\,\delta\,(x-x_g, y, z-d_g) \quad , \tag{5-1}$$

where D is the diffusion constant, τ is the lifetime, and g is the generation rate of electron-hole pairs.

If the thickness w between the potential barrier and the ohmic contact is much greater than L , and the other boundaries in the y and z directions are both much further away from the generation source, EBIC is calculated under the following boundary conditions as discussed in §3-2.

$$D \left.\frac{\partial p}{\partial z}\right|_{z=0} = s\, p\Big|_{z=0} \quad , \tag{5-2a}$$

$$p\Big|_{x=0} = 0 \text{ (at the Schottky barrier)} \ , \tag{5-2b}$$

$$p\Big|_{x=+\infty} = 0 \quad , \tag{5-2c}$$

where s is the surface recombination velocity.

Once the distribution p is known, EBIC can be found as follows.

$$j = eD\int_{0}^{+\infty}\int_{-\infty}^{+\infty} \left.\frac{\partial p}{\partial x}\right|_{x=0} dy\, dz \quad , \tag{5-3}$$

where e is the charge of an electron. Berz et al. [2] solved the diffusion equation (5-1) under the boundary conditions (5-2a), (5-2b) and (5-2c) by the mirror image method. In addition to the real source at x_g, an image sink was introduced at the symmetric position $-x_g$ with respect to the Schottky barrier (see Fig. 5-2). When the material extends to $x=\pm\infty$, the solution of eq.(5-1) is given by p[x] ($x=\pm x_g$). When the Schottky barrier is introduced, the minority carrier distribution is expressed as $p[x_g] + p[-x_g]$ in order to satisfy the boundary condition (5-2b, $p|_{x=0}=0$), and j is obtained as follows.

$$J\ (x_g) = \frac{j}{eg} = \frac{2}{\pi} X_g \left\{ \int_0^{D_g} \frac{K_1(\sqrt{X_g^2+T^2})}{\sqrt{X_g^2+T^2}}\, dT \right.$$
$$\left. + \int_{D_g}^{+\infty} \exp(-S(T-D_g))\, \frac{K_1(\sqrt{X_g^2+T^2})}{\sqrt{X_g^2+T^2}}\, dT \right\} \tag{5-4}$$

where $X_g=x_g/L$, $D_g=d_g/L$, $S=s/(L/\tau)$, and T is the variable for integration. The value of $J(x_g)$ is normalized to be unity when all the generated carriers contribute to EBIC. The function $K_1(\sqrt{X_g^2+T^2})$ is the second-modified first-order Bessel function.

For the analysis of EBIC considering sample dimensions we take the fundamental case that the diffusion length is comparable with or larger than the thickness w (see Fig. 5-1).

Then, one must use the following boundary condition instead of (5-2c).

$$p\Big|_{x=w} = 0 \quad \text{(at the ohmic contact)} \quad . \tag{5-2c'}$$

The solution of eq. (5-1) under the boundary conditions (5-2a), (5-2b) and (5-2c') can be obtained by extending the mirror image method proposed by Berz [2] and Opdorp [3]. In addition to the real source at x_g, a family of virtual image sources and sinks are introduced at the symmetric positions with respect to the barrier and the ohmic contact (see Fig. 5-2). Open and solid circles represent the sources and sinks, respectively. Therefore, the sources are at x_g, $2w+x_g$, $4w+x_g$,····· and $-(2w-x_g)$, $-(4w-x_g)$,·····, and the sinks are at $-x_g$, $-(2w+x_g)$, $-(4w+x_g)$,····· and $2w-x_g$, $4w-x_g$, ·····, respectively. When the material extends to $x=\pm\infty$, the solution of eq.(5-1) is given by $p[x]$ ($x=\pm x_g$, $\pm(2w-x_g)$, $\pm(2w+x_g)$,·····) (see Fig. 5-2). If the influence of ohmic contact must be taken into account, the minority carrier distribution is expressed using the following infinite series in order to satisfy the boundary conditions (5-2b, $p\big|_{x=0}=0$) and (5-2c', $p\big|_{x=w}=0$).

$$\begin{aligned} p^*[x_g] &= p[x_g] \quad + p[-x_g] \\ &+ p[2w-x_g] + p[-(2w-x_g)] \\ &+ p[2w+x_g] + p[-(2w+x_g)] \\ &+ \text{- - - - - - - - -} \quad , \end{aligned} \tag{5-5}$$

The induced currents by pairs of sources and sinks, i.e. $p[x_g]$ and $p[-x_g]$, $p[2w-x_g]$ and $p[-(2w-x_g)]$, $p[2w+x_g]$ and $p[-(2w+x_g)]$, ····· are expressed by $J(x_g)$, $-J(2w-x_g)$, $J(2w+x_g)$, ·····, respectively, with the aid of eq. (5-4). Then, the total EBIC is expressed in the infinite series as follows.

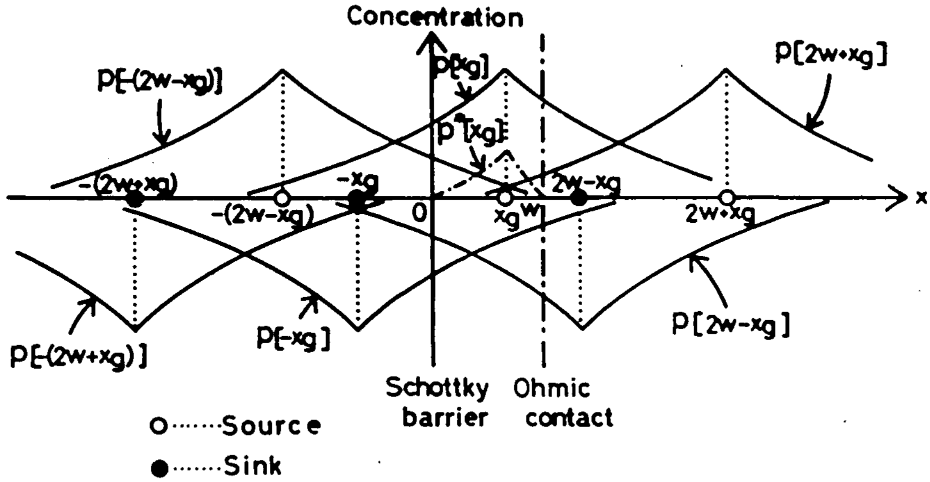

Fig. 5-2 Schematic view of excess minority carrier concentration pattern for each source and sink which are represented by the open and solid circles, respectively.

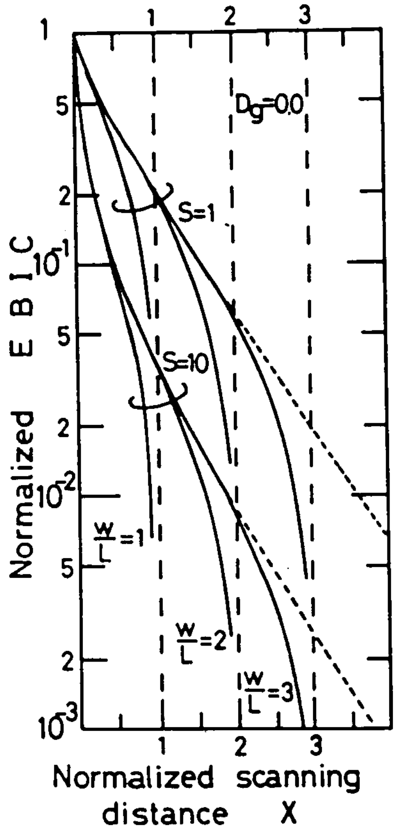

Fig. 5-3

Dependence of EBIC on the normalized scanning distance X(≡x/L); full and broken curves are for the cases with and without the influence of ohmic contact, respectively. The normalized sample width w/L is 1.0, 2.0 and 3.0, and the normalized generation depth D_g is 0.0. The values of the surface recombination velocity parameter S (see text) are 1 and 10 for upper and lower group of curves, respectively.

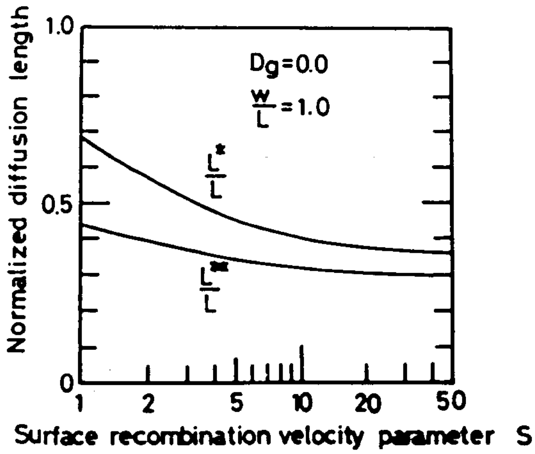

Fig. 5-4

Estimated diffusion length from the reciprocal gradient of the curve at the center of the scanning distance in the case of D_g=0.0 and w/L=1.0; S varies from 1 to 50. L* and L** are for the cases without and with the influence of ohmic contact, respectively.

$$J^*(x_g) = J(x_g) - J(2w-x_g) + J(2w+x_g) \\ - J(4w-x_g) + J(4w+x_g) \\ - - - - - - - - - \quad . \qquad (5\text{-}6)$$

The value of J^* converges to a certain value, and can be calculated by a computer in cases of any values of w, L and S.

In Fig. 5-3, the logarithm of J^* is plotted by solid lines as a function of X (=x/L) when w/L is 1.0, 2.0 and 3.0, and D_g is 0.0. The dashed lines are for the case without the influence of ohmic contact. The upper and lower curves are for S=1 and 10, respectively. The values of $\log J^*$ decrease superlinearly within one diffusion length away from the barrier. Therefore, one makes considerable errors if one estimates the value of L from the reciprocal gradient of the curve at arbitrary X. In order to show an extreme example, we consider the case of w/L=1.0 and D_g=0.0. The reciprocal gradient of the curve in the linear region at X=0.5 without and with the influence of ohmic contact are put as L^* and L^{**}, respectively. The values of L^* and L^{**} thus obtained are plotted as a function of S in Fig. 5-4. When S is unity, L^* is about 68 % of L, and L^{**} is about 44 % of L. The values of L^* and L^{**} reduce to only about one third of L when S is 50.

The method of the analysis for a point source mentioned above can be easily applied to the finite generation distribution by the dividing method discussed in Chapters III and IV. Especially in the cases of light-emitting diodes (LED's) and laser diodes (LD's) using GaAs and GaP, the dimension of the generation region is the order of μm for V_a=20 ∿ 30 kV, and is comparable with the thickness of the epitaxial layers. Therefore, the dividing method becomes an effective means to measure L and s in the epitaxial layers.

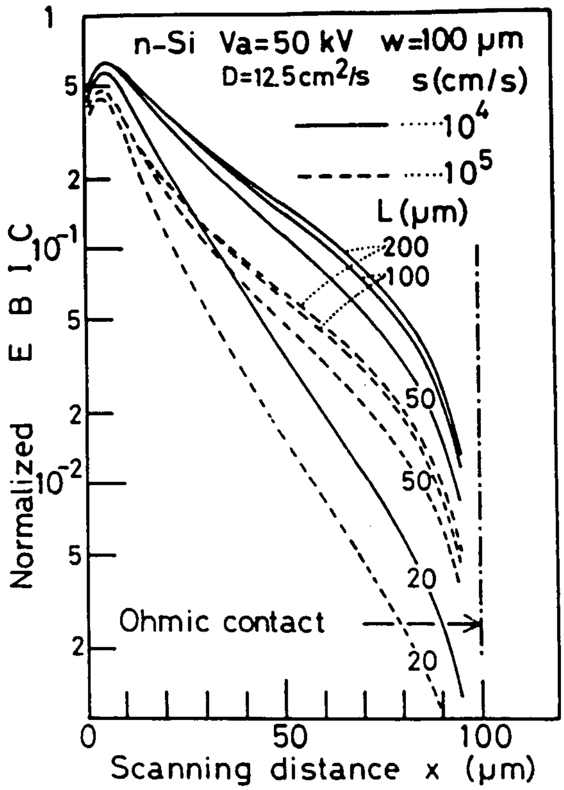

Fig. 5-5 Dependence of EBIC on the scanning distance x for n-Si Schottky diodes. The length w between the barrier and the ohmic contact is 100 μm, the accelerating voltage V_a is 50 kV, and L is 20 ∿ 200 μm. Solid and broken lines are for $s=10^4$ and 10^5 cm/sec, respectively, taking the generation distribution into account. The diffusion constant D of holes is 12.5 cm^2/sec.

5-3. Application to Si

The diffusion length in the Si bulk material used for solar cells or LSI's is comparable with the dimensions of each element. And so, the minority carrier distribution is affected very much by element dimensions. The Schottky diode was taken for a fundamental model to reveal the influence of sample dimensions.

Calculated EBIC's by the dividing method in the case of n-Si for w=100 μm and V_a=50 kV are shown in Fig. 5-5. The diffusion constant D of holes is taken as a typical value of 12.5 cm^2/sec. Solid and dashed lines are for s=10^4 and 10^5 cm/sec, respectively, and L is 200, 100, 50 and 20 μm for the curves from upper to lower in each group. The generation source is assumed to be a semi-sphere. The number of the generated electron-hole pairs at any point in the semi-sphere is proportional to $\exp(-4.0(r/R)^2)$ (r: the distance between the point and the center d_g, R: the radius of the semi-sphere). The generation distribution is assumed in order that the depth dose function along the z-axis agrees with that proposed by Everhart [4], and the values of d_g and R are 5 μm and 11 μm, respectively, for V_a=50 kV.

As shown in Fig. 5-5, the absolute value of EBIC increases with decreasing s for the same L value. The curves converge to a certain curve for both s=10^4 and 10^5 cm/sec when L becomes greater than w. For convenience, the logJ*vs. x curves are divided into three parts, i.e. A) near the barrier ($0 \leqq x \leqq 30$ μm), B) middle range ($30 \leqq x \leqq 70$ μm) and C) near the ohmic contact ($70 \leqq x \leqq 100$ μm). In the region A), peaks appear at x=6 μm owing to the edge effect described in §3-3, and logJ* decreases superlinearly because of the surface recombination effect. In the region C), logJ* decreases

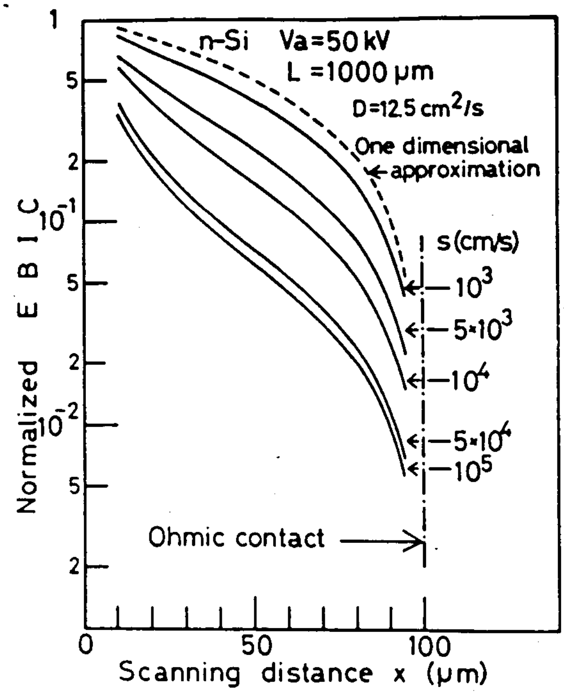

Fig. 5-6 Dependence of EBIC on the scanning distance x for n-Si when L is much greater than w. The solid lines are results by the three-dimensional solutions for $s=10^3$, 5×10^3, 10^4, 5×10^4 and 10^5 cm/sec, respectively. The dashed line is EBIC by one-dimensional approximation; V_a=50 kV, w=100 μm and L=1000 μm.

rapidly because the ohmic contact is a carrier sink. In the middle range B), $\log J^*$decreases almost linearly. The reciprocal gradient of the curve increases as L becomes large in the range of $L \leqq 100$ μm. The gradients of the curves are not so affected by surface recombination. If V_a is lowered to 10 kV, the surface recombination affects EBIC much more than for V_a=50 kV, because the generation depth becomes shallower. In fact, the gradients of the curves in region A) are steeper than those for V_a=50 kV for the same L values. Therefore, in the case of $L \leqq 100$ μm, L and s can be determined mainly from the slopes of the linearly decreasing region for high V_a (50 kV in this work) and the superlinearly decreasing region near the Schottky barrier for low V_a (10 kV in this work), respectively, taking the influence of ohmic contact into account. But, in the case of $L \geqq 100$ μm, the value of L cannot be determined definitely because the slope of the curve in the linearly decreasing region does not change even if L varies.

When L becomes much larger than w, the curves of EBIC vs. x converge to a certain curve. Calculated EBIC's in the case of n-Si for V_a=50 kV, w= 100 μm and L= 1000 μm are shown by solid lines in Fig. 5-6 for s=10^3, 5×10^3,10^4, 5×10^4 and 10^5 cm/sec, respectively. The generation source is assumed to be a point at the depth d_g. The dashed line is a solution of one-dimensional approximation (see appendix in this chapter). The absolute value of EBIC becomes larger with decreasing s, and the curve for $s\to0$ cm/sec approaches to the solution of one-dimensional approximation. It can be explained as follows. In the case of s=0 cm/sec, there is no carrier recombination at the surface. Hence, the material can be considered to extend to $z=-\infty$ by introducing an image source at $(x_g,0,-d_g)$. EBIC is obtained by integrating dp/dx in the y-z plane at x=0. And so,the EBIC by the point source at $(x_g,0,\pm d_g)$ using

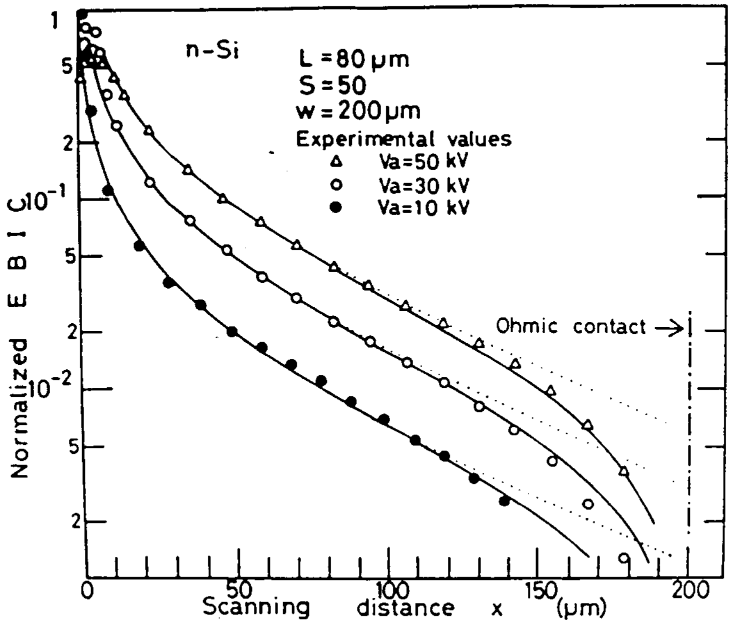

(a)

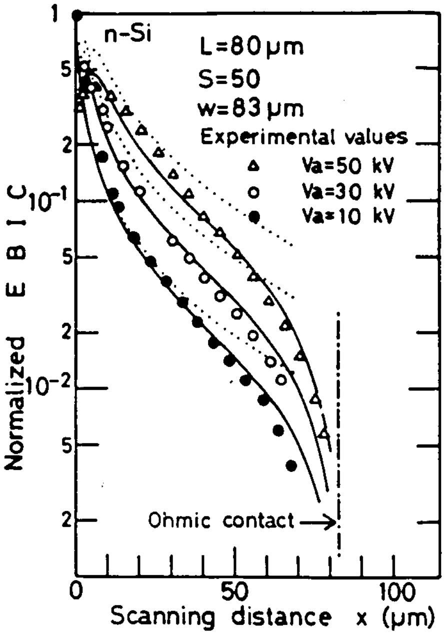

(b)

Fig. 5-7 Experimental results in Si Schottky diodes for w=200 µm and 83 µm in figures (a) and (b), respectively. Va is 10, 30 and 50 kV. Solid and dotted lines are theoretical results for L= 80 µm and S=50 with and without the influence of ohmic contact, respectively.

the three-dimensional diffusion equation becomes identical to that derived by one-dimensional diffusion equation considering the planar source at $x=x_g$ in the y-z plane [5]. However, in practice, Si has a finite value of s and so, the three-dimensional solution must be needed in the case of $L \geqq w$. The value of s can be determined from the absolute value of EBIC following the discussion of §4-2 using the electron-hole pair creation energy E_{pc} by an electron beam.

The experimental results in Si Schottky diodes with w=200 μm and 83 μm made from one wafer are shown in Figs. 5-7 (a) and 5-7 (b),respectively. Sample preparations and measurement procedures have been already shown in §3-4. The results of the theoretical calculation using L=80 μm and S=50 for three different V_a's (10, 30 and 50 kV) are shown by solid lines in both figures. The results of the theoretical calculation without the influence of ohmic contact are shown by dotted lines in Fig. 5-7.
In the case of w=200 μm, the sample width is three times larger than L, and so the slope of the linear region ($50 \leqq x \leqq 120$ μm) is not very changed by the influence of ohmic contact. In the case of w=83 μm, the curves are quite different from those for w=200 μm, and the reciprocal gradient of the curves in the middle range ($25 \leqq x \leqq 55$ μm) gives L=20 μm which is a quarter of the real diffusion length. Both in Figs. 5-7 (a) and (b), theoretical calculations show good agreement with the experimental results, which shows that the method discussed in §5-2 is an effective means to analyze the effect of sample dimensions.

5-4. Summary

The minority carrier distribution is affected very much by the length w between a potential barrier and an ohmic contact if w is equal to or shorter than the diffusion length L. The dependence of EBIC J^* on the scanning distance x was investigated by extending the mirror image method.

In the case of $w/L \geqq 1$, $\log J^*$ decreases almost linearly in the middle range of the scanning distance, but the estimated diffusion length from the curves is much shorter than the real diffusion length (e.g. 30 to 44 % in the case of L=w). The values of L and s can be determined mainly from the slopes of the curves for high and low V_a, respectively, taking the influence of ohmic contact into account.

In the case of $w/L < 1$, the slope of the linearly decreasing region of $\log J^*$ vs. x curves does not change even if L varies. The dependence of EBIC on x converges to a certain curve. The value of L cannot be determined definitely, but the value of s can be obtained from the absolute value of EBIC.

The experimental results in Si Schottky diodes agreed fairly well with the theory, which showed that the extended mirror image method was effective in analyzing EBIC considering the sample dimensions.

References

[1] Oldwig von Roos: Solid-State Electron. 21 , 1063 (1978)

[2] F. Berz and H. K. Kuiken: Solid-State Electron. 19 , 437 (1976)

[3] C. van Opdorp: Philips Res. Rep. 32 , 192 (1977)

[4] T. E. Everhart and P. H. Hoff: J. Appl. Phys. 42 ,5837 (1971)

[5] W. H. Hackett, Jr.: J. Appl. Phys. 43 , 1649 (1972)

Appendix. One-dimensional approximation

If the diffusion length L is infinitely long, minority carriers do not recombine until they flow into the barrier or the ohmic contact. Therefore, the diffusion current does not vary spatially. The minority carrier distribution p can be expressed as a linear function of x in the case of one-dimensional approximation. If the point source g is located at x_g, p(x) is put as follows.

$$p(x) = ax + b \qquad (a>0,\ 0 \leqq x \leqq x_g) \quad , \tag{5-A1}$$

$$p(x) = cx + d \qquad (c<0,\ x_g \leqq x \leqq w) \quad . \tag{5-A2}$$

The factors a, b, c and d can be determined from the following conditions.

$$p(0) = 0 \quad , \tag{5-A3}$$

$$p(w) = 0 \quad , \tag{5-A4}$$

$$ax_g + b = cx_g + d \quad , \tag{5-A5}$$

$$\left| D \left.\frac{dp}{dx}\right|_{x=0} \right| + \left| D \left.\frac{dp}{dx}\right|_{x=w} \right| = g \quad . \tag{5-A6}$$

The eq.(5-A5) shows the continuity condition at $x=x_g$, and the eq. (5-A6) gives that all the generated carriers flow into the Schottky barrier and the ohmic contact without recombination in materials. The solution p(x) becomes as follows.

$$p(x) = \frac{g}{D}\left(1 - \frac{x_g}{w}\right) x \qquad (0 \leqq x \leqq x_g) \quad , \tag{5-A7}$$

$$p(x) = \frac{g}{D}\frac{x_g}{w}(w - x) \qquad (x_g \leqq x \leqq w) \quad . \tag{5-A8}$$

Normalized EBIC J*is expressed by

$$J^* = \frac{1}{eg}\, eD \left.\frac{dp}{dx}\right|_{x=0} = 1 - \frac{x_g}{w} \quad . \tag{5-A9}$$

VI . DETERMINATION OF LIFETIME AND DIFFUSION CONSTANT BY PHASE SHIFT TECHNIQUE

6-1. Introduction

Accurate determination of lifetime τ of minority carriers is very important in characterizing semiconducting materials. The value of τ can be measured directly from the transient response after the injection of minority carriers. The radiative recombination lifetime was measured in GaP and GaAs from the decay of photoluminescence [1], cathodoluminescence [2] or electroluminescence[3]. The photoconductance decay method [4] is the most commonly used technique to measure lifetime including radiative and non-radiative processes. In these methods, measurement of τ in small area of the order of μm^2 is very difficult because the sample surface must be relatively wide in order to obtain a sufficient signal. The spatial variation of τ could be determined from the decay of the electron beam induced current (EBIC) using a scanning electron microscope (SEM) [5-8]. The value of τ is much influenced by surface recombination since light or an electron beam for excitation enters through the surface.

The value of τ can be obtained from the diffusion length L using the relation $L=\sqrt{D\tau}$. The value of L can be determined by the spectral response method using solar cells [9], or by the surface photovoltaic method [10]. In both methods, the accurate absorption coefficient must be needed to determine the value of L. As discussed in Chapters II $\sim$ V, the EBIC method using SEM is a very convenient technique to measure L in small area of the order of μm^2, and there have been many theoretical [11-14] and experimental [15-16] works up to date. In the method,however, the diffusion constant D must be given in order to obtain τ.

When the intensity of excitation for electron-hole pair generation is modulated, the phase of luminescence or induced current is shifted from that of the excitation source because of the recombination of injected minority carriers in a material. The value of τ can be determined from the amount of the phase shift. Hwang [17] obtained τ in GaAs from the phase shift of photo-luminescence. In the method, the phase shift is influenced by the surface recombination velocity and the absorption coefficient which affect minority carrier distribution very much. Reichl et al. measured τ in Si [18-20] and GaAs [21] using the phase shift in photo-induced current. Munakata [22] and Othmer [23] measured τ by the phase shift of EBIC in Ge and Si, respectively. They used the solution of the one-dimensional diffusion equation without any consideration of the surface recombination effect.

If such a phase shift method is combined with the conventional line scan method of EBIC (i.e. measurement of L using DC electron beam), the lifetime and the diffusion constant of minority carriers in small area can be determined simultaneously. Kamm et al. [24] determined τ and D in Si. They made a Schottky barrier with a silver paint on Si surfaces, and measured EBIC by scanning the electron beam on the surface parallel to the barrier. In that method, surface preparation has much effect on τ [25], and the configuration used by them is not convenient when one measures τ and D in materials with small L. The analysis is very complicated, and Roos pointed out errors in their analysis [26], and suggested a simple configuration [27].

In this chapter, we take the configuration that the electron beam scans on the surface perpendicular to the barrier plane. With this configuration, the time-dependent diffusion equation can be simply reduced to the steady-state diffusion equation, and the complication in the analysis that Roos indicated [26] can be excluded. This phase shift method can be applied to materials with small L. We solve the three-dimensional time-dependent diffusion equation taking the surface recombination effect into account, and clarify the relation of τ and the phase shift theoretically. We show that three-dimensional solutions can be expressed by one-dimensional solutions with empirical correction factors, and that τ and D can be determined without any restriction for modulation frequency. Experimental results in Si are also shown.

6-2. Relation between lifetime and phase shift

We take a Schottky diode as shown in Fig. 6-1 for simple theoretical calculation. We assume a point generation source which has time-variable part $\Delta g e^{i\omega t}$ ($\omega=2\pi f$, ω:angular frequency, f:modulation frequency) at $(x_g, 0, d_g)$. When the time-variable part of the number of minority carriers is put as $\bar{p}^* e^{i\omega t}$ ($\bar{p}^*$ is a complex variable), $\bar{p}^*$ satisfies the conventional steady-state diffusion equation by introducing the complex effective diffusion length L^*_{eff} ($\equiv L/\sqrt{1+i\omega\tau}$; $L=\sqrt{D\tau}$). If the time-variable part of EBIC is put as $\bar{j}^* e^{i\omega t}$ ($\bar{j}^*$ is complex EBIC), $\bar{j}^*$ can be expressed as follows by the mirror image method as discussed in §3-2.

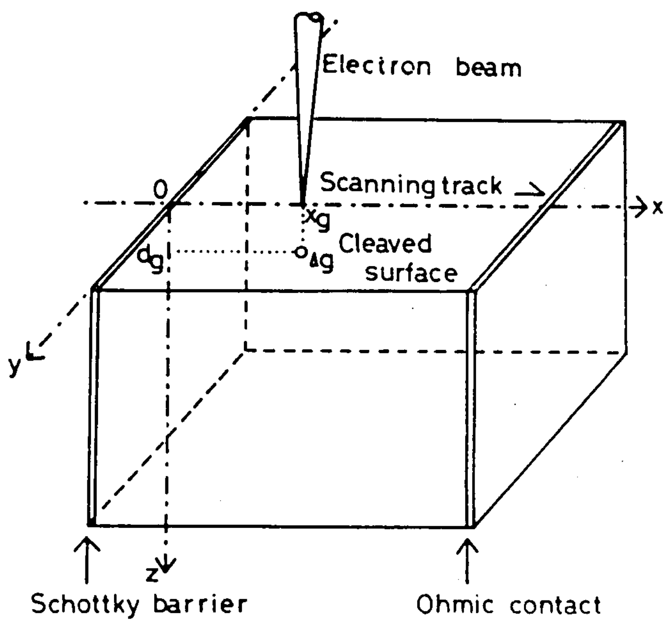

Fig. 6-1 Schematic view of experimental conditions and definition of the co-ordinate system.

$$\frac{\bar{j}^*}{e\Delta g} = \frac{2}{\pi} \frac{x_g}{L^{*2}_{eff}} \left[\int_0^{d_g} K_1 \left(\frac{\sqrt{x_g^2 + T^2}}{L^*_{eff}} \right) \frac{L^*_{eff}}{\sqrt{x_g^2 + T^2}} \, dT \right.$$

$$\left. + \int_{d_g}^{+\infty} \exp\left(- \frac{s(T-d_g)}{D}\right) K_1\left(\frac{\sqrt{x_g^2 + T^2}}{L^*_{eff}}\right) \frac{L^*_{eff}}{\sqrt{x_g^2 + T^2}} \, dT \right], \quad (6\text{-}1)$$

where e is the charge of an electron, s is the surface recombination velocity and T is the variable for integration. The function K_1 is the second-modified first-order Bessel function with complex variables. The absolute value of EBIC $\Delta\eta$ and the phase shift ϕ from the source are given as follows.

$$\Delta\eta = \left| \frac{\bar{j}^*}{e\Delta g} \right| , \quad (6\text{-}2)$$

$$\phi = \tan^{-1} \left(\frac{\mathrm{Im}\ \bar{j}^*}{\mathrm{Re}\ \bar{j}^*} \right) , \quad (6\text{-}3)$$

where Re and Im stand for real and imaginary parts, respectively. The value of $\Delta\eta$ is normalized to be unity when all the variable part Δg contribute to the variable part of EBIC. Since $\bar{j}^*$ is a function of τ, the value of ϕ becomes a function of τ. The values of $\Delta\eta$ and ϕ can be calculated numerically. We assume a point source for simple calculation, but the method mentioned above can be easily applied to the finite generation distribution by the dividing method described in Chapters III and IV .

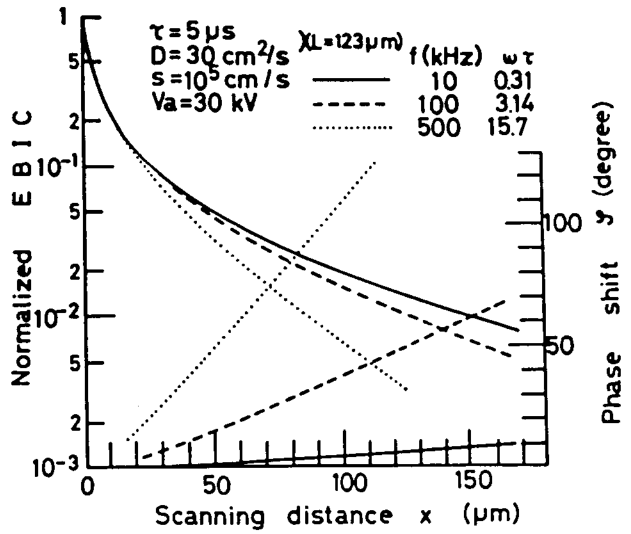

Fig. 6-2 Normalized intensity and phase shift of EBIC vs. scanning distance x curves. The concave curves and the almost linear lines are for the intensity (left axis) and the phase shift (right axis), respectively. The solid, broken and dotted lines are for f=10, 100 and 500 kHz (i.e. $\omega\tau$=0.31, 3.14 and 15.7), respectively. Lifetime τ is taken as 5 μs. The diffusion constant D is 30 cm^2/sec, and the surface recombination velocity s is 10^5cm/sec.

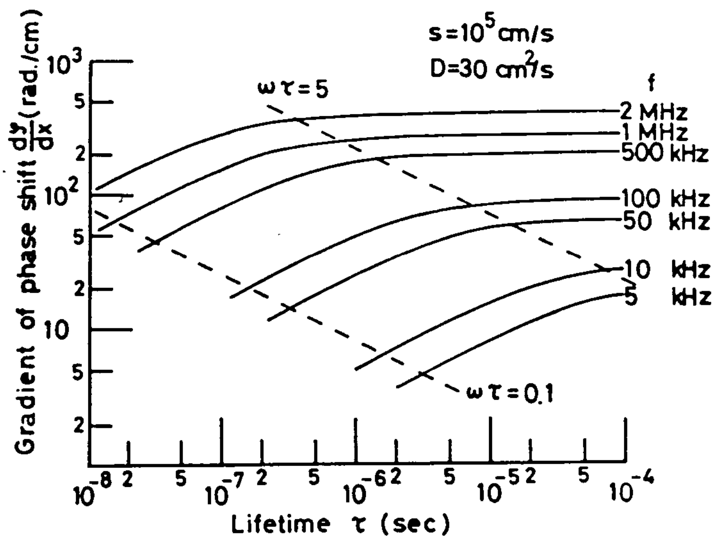

Fig. 6-3 Dependence of gradient of phase shift $d\phi/dx$ on τ; D= 30 cm^2/sec and s= 10^5 cm/sec.

The values of $\Delta\eta$ and ϕ were calculated as a function of scanning distance x for p-Si as an example. The results are shown in Fig. 6-2, when τ is put as a typical value of 5 μs. In the figure, the concave curves and the almost linear lines are for $\Delta\eta$ - x and ϕ - x relations, respectively. The solid, broken and dotted lines are for f=10, 100 and 500 kHz (i.e. $\omega\tau$ = 0.31, 3.14 and 15.7), respectively. The diffusion constant D is put as 30 cm^2/sec. The surface recombination velocity s is taken as 10^5 cm/sec, since the ordinary surface recombination velocity of Si is $10^3 \sim 10^5$ cm/sec. The accelerating voltage is put as 30 kV. The point source is assumed to be located at the maximum energy dissipation depth of about 3 μm under the surface based on Kanaya's model [28] for electron-hole pair generation distribution.

In the case of $\omega\tau < 0.1$, the dependence of $\Delta\eta$ on x agrees with that measured by a conventional line scan method using DC electron beam. The value of L can be determined from the slope of the $\Delta\eta$ - x curves taking the surface recombination effect into account as discussed in Chapter III. The value of L^*_{eff} almost equal to L, and so ϕ becomes nearly zero.

In the case of $\omega\tau \geqq 0.1$, ϕ increases almost linearly with x over the range of $x \geqq L$, and the gradient $d\phi/dx$ becomes large with increasing f as shown in Fig. 6-2. The gradient $d\phi/dx$ is found to increase as τ becomes large for the same f value, and not to change even if s varies from 10^2 to 10^5 cm/sec from the calculation for various parameters. Figure 6-3 shows the dependence of $d\phi/dx$ on τ, when f is varied from 5 kHz to 2 MHz. The values of D and s are 30 cm^2/sec and 10^5 cm/sec, respectively. For each value of f, $d\phi/dx$ increases monotonously with τ within the range of $0.1 \leqq \omega\tau \leqq 5$, and approaches to a certain value asymptotically over the range of $\omega\tau \geqq 5$.

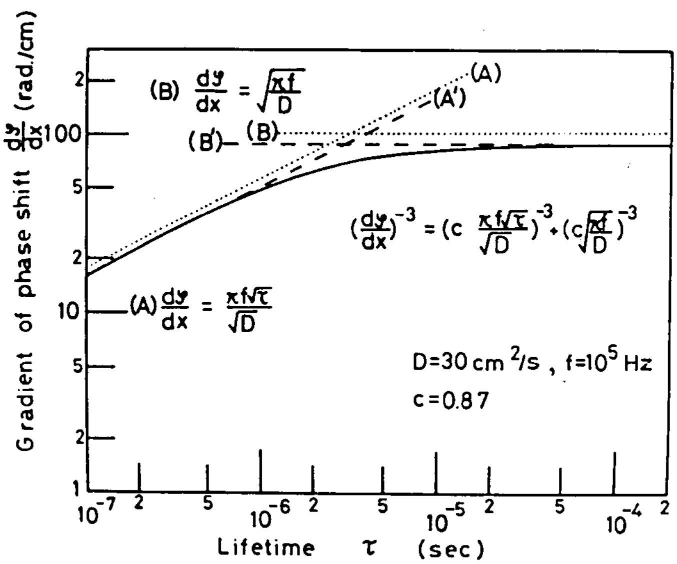

Fig. 6-4 Expression of the dependence of $d\phi/dx$ on τ using the approximated solutions of the one-dimensional diffusion equation in the case of D= 30 cm^2/sec and f= 10^5 Hz. Solid line is a three-dimensional solution. Lines (A) and (B) are the approximated one-dimensional solutions, and (A') and (B') are the asymptotes for the three-dimensional solution. The correction factor c for the three-dimensional solution is 0.87.

If we take the solutions of the one-dimensional diffusion equation, $d\phi/dx$ is given as follows [24].

$$\frac{d\phi}{dx} = \frac{L\omega}{2D} = \frac{\pi f\sqrt{\tau}}{\sqrt{D}} \qquad (\omega\tau \ll 1) \quad , \qquad (6\text{-}4)$$

or

$$\frac{d\phi}{dx} = \sqrt{\frac{\omega}{2D}} = \sqrt{\frac{\pi f}{D}} \qquad (\omega\tau \gg 1) \quad . \qquad (6\text{-}5)$$

Following the three-dimensional solution (eqs.(6-1), (6-2) and (6-3)) as shown in Fig. 6-3, $d\phi/dx$ increases proportionally to $\sqrt{\tau}$ in the range of $\omega\tau < 0.5$, and reaches to a certain value over the range of $\omega\tau > 5$, which can be explained qualitatively by eqs. (6-4) and (6-5), respectively. The $d\phi/dx$ vs. τ curves in Fig. 6-3 can be represented by one function with the combination of the approximated solutions of the one-dimensional diffusion equation (eqs. (6-4) and (6-5)). We show an example in the case of $f=10^5$ Hz and $D=30$ cm^2/sec in Fig. 6-4. The solid line is the three-dimensional solution from Fig. 6-3, and the dotted lines (A) and (B) express eqs. (6-4) and (6-5), respectively. The broken lines (A') and (B') show the asymptotic solutions of the three-dimensional solution in the ranges of $\omega\tau < 0.5$ and $\omega\tau > 5$. The absolute values of (A') and (B') become about 87 % of those of (A) and (B) based on the results of calculation. As shown in Fig. 6-4, the three-dimensional solution is given by a combination of the lines (A') and (B'), and is expressed as follows.

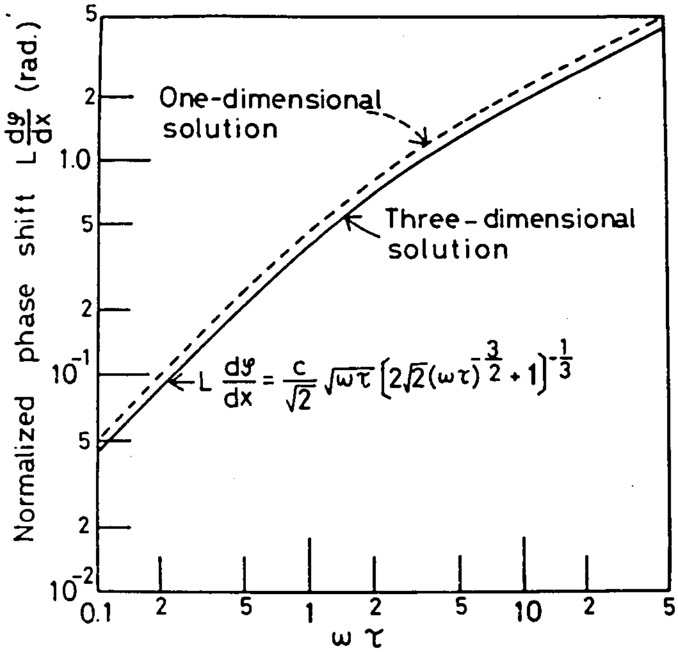

Fig. 6-5 Normalized phase shift $Ld\phi/dx$ vs. $\omega\tau$ curves. Solid line is a three-dimensional solution expressed by the approximated one-dimensional solutions with empirical correction factors. Broken line is the one-dimensional solution.

$$\left(\frac{d\phi}{dx} \right)^{-n} = \left(c \frac{\pi f \sqrt{\tau}}{\sqrt{D}} \right)^{-n} + \left(c \sqrt{\frac{\pi f}{D}} \right)^{-n} , \qquad (6-6)$$

where n is a positive integer. We calculated eq. (6-6) in the cases of n=1 ∿ 5, and determined n as 3 in order that the solid curve in Fig. 6-4 can be well represented by eq. (6-6). The value of c is the correction factor for the three-dimensional solution, and c is about 0.87 as mentioned above.

From, eq. (6-6), we can derive the following relation using the conventional diffusion length L.

$$L \frac{d\phi}{dx} = \frac{c}{\sqrt{2}} \sqrt{\omega\tau} \left\{ 2\sqrt{2} \, (\omega\tau)^{-\frac{3}{2}} + 1 \right\}^{-\frac{1}{3}} . \qquad (6-7)$$

The term $Ld\phi/dx$ is considered to be the normalized phase shift which is the amount of the phase shift when the electron beam scans over one diffusion length. It should be noted that $Ld\phi/dx$ is a function of only $\omega\tau$. Figure 6-5 shows the dependence of $Ld\phi/dx$ on $\omega\tau$ by the solid line. If the values of L and $d\phi/dx$ are known, τ can be determined from the curve for any modulation frequency, and D is also obtained by the relation of $L=\sqrt{D\tau}$. The modulation frequency f can be chosen freely, and the restrictions of $\omega\tau< 0.5$ or $\omega\tau> 5$ for the approximation need not to be taken into account.

The phase shift derived by McKelvey [29] using the one-dimensional diffusion equation is shown by the dashed line in Fig. 6-5. The estimated value of $\omega\tau$ by the one-dimensional solution is about 76 ∿ 87 % of that by the three-dimensional solution for every value of $Ld\phi/dx$. In the case of the one-dimensional solution , L is determined directly from the gradient of the linearly decreasing region of EBIC curve, and is about 60 ∿ 80 % of the real value from the results of the detail analysis taking the surface recombination effect into account [14]. Therefore, the value of $\omega\tau$ derived by the one-dimensional solution is only 30 ∿ 70 % of the real value, because $\omega\tau$ decreases proportionally to L and L^2 in the regions of $Ld\phi/dx < 0.3$ and $Ld\phi/dx > 2$, respectively. One must use the three-dimensional solution in order to determine the accurate value of τ.

6-3. Experimental results in Si

A conventional SEM was used for the primary electron beam which was modulated at 1 ∿ 50 kHz with the duty of 0.5 by a chopping coil inserted into the beam path. The beam current was as low as 10^{-10} A. The maximum minority carrier density in this experiment was considered to be about 3×10^{14} cm^{-3}, and the low injection condition was satisfied. The induced current was measured by the voltage drop across the load resistance which was connected to the Schottky barrier with an ohmic contact. The signal had a rectangular wave form owing to the chopped primary electron beam, and so the fundamental frequency component in the Fourier series of the signal was detected by an auto-phase lock-in amplifier. The EBIC $\Delta\eta$ and the phase shift ϕ from the source were recorded simultaneously.

The diffusion length L is determined in the case of $\omega\tau < 0.1$ taking the surface recombination effect into account. The dependence of $\Delta\eta$ on x agrees with that measured by a conventional line scan method using DC electron beam as discussed in §6-2.

When V_a is low, giving the shallow generation depth, surface recombination has a large effect on EBIC. When V_a is high, giving the deep generation depth, the surface recombination effect is reduced. The accurate value of L could be determined by fitting experimental data to theoretical curves for both low and high V_a's (10 and 50 kV, respectively, in this work) as shown in §3-3.

The value of $d\phi/dx$ is obtained at an appropriate modulation frequency which satisfies $\omega\tau > 0.1$. At high V_a, the surface recombination effect is reduced, and so we chose the highest V_a (30 kV in this work) as far as the electron beam could be chopped. Once the values of L and $d\phi/dx$ are known, the values of τ and D can be determined from the curve in Fig. 6-5.

Samples were p- and n-type Si with the resistivity ρ of 10 and 0.1 Ω cm, respectively. Ohmic contacts were made by evaporating gallium-doped gold and antimony-doped gold on to the p- and n-type samples, respectively. Schottky contacts were made by evaporating aluminium and gold on to the p- and n-type samples, respectively, in a vacuum as low as 10^{-7} Torr. The samples were inserted into a vacuum chamber for EBIC measurement immediately after they were cleaved.

The diffusion length L in p-type Si was determined as 130 μm from the $\Delta\eta$ - x curves in the case of $\omega\tau < 0.1$. The experimental results of the phase shift method are shown in Fig. 6-6 by solid lines for f=5, 10, 20, 30 and 50 kHz,respectively. The phase shift increases with x almost linearly as described in §6-2. The values of τ were determined using Fig. 6-5 as 9.5, 9.5, 8.8, 8.6 and 8.3 μs from the gradients of the lines in Fig. 6-6 for 5, 10, 20, 30 and 50 kHz, respectively. The obtained values of τ show little difference with each other in any measurement

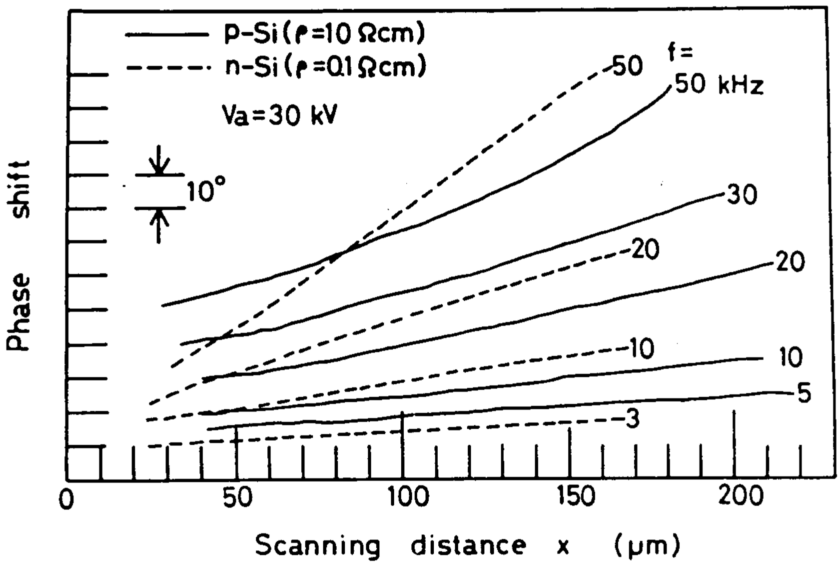

Fig. 6-6 Experimental results of the phase shift method in p-(ρ=10 Ωcm) and n-type (ρ=0.1 Ωcm) Si.

condition from $\omega\tau$=0.3 (at f=5 kHz) to 3.0 (at f=50 kHz) . It proved that the modulation frequency could be chosen freely as mentioned in §6-2. If we take the averaged value of τ (i.e. τ=8.9 μs), the diffusion constant D of electrons was determined as 19 cm^2/sec which almost agreed with the reported value [30]. The slight deviation from the straight line for f=50 kHz may come from unstableness of the chopped beam, because the chopping coil used in our experiment was not designed for high frequency modulation above 50 kHz.

The diffusion length in n-Si was obtained as L= 80 μm, and the phase shifts are shown in Fig. 6-6 by broken lines for f=3, 10, 20 and 50 kHz, respectively. The determined values of τ from the gradients of the lines were 8.8, 9.2, 9.2 and 10.5 μs for f=3, 10, 20 and 50 kHz, respectively. The values of τ almost equal with each other as in the case of p-Si. If we take the averaged value of τ (i.e. τ=9.4 μs), the diffusion constant D of holes becomes 7 cm^2/sec which also agrees with the reported value [30].

The generation distribution is considered to be a semi-sphere the radius of which is about 6 μm at V_a=30 kV using the Kanaya's model [28]. The dimensions of generation distribution are sufficiently small in comparison with the diffusion length of the samples. Therefore, the point source assumption in the analysis is reasonable.

6-4. Summary

When the intensity modulated electron beam is used, the phase of induced current (EBIC) is shifted from that of excitation source because of the recombination in materials. We solved the three-dimensional time-dependent diffusion equation taking the surface recombination effect into account, and clarified the relation of τ and the phase shift ϕ theoretically.

In the case of $\omega\tau \geqq 0.1$, ϕ increases almost linearly with x over the range of $x \geqq L$. The gradient $d\phi/dx$ becomes a function of τ and is not affected by surface recombination. The relation of $d\phi/dx$ on τ was found to be expressed using the approximated solutions of the one-dimensional diffusion equation with the empirical correction factors. The normalized phase shift $Ld\phi/dx$ becomes a function of only $\omega\tau$. If the values of L and $d\phi/dx$ are known, τ and D are determined with the aid of $Ld\phi/dx$ vs. $\omega\tau$ curve without any restriction for modulation frequency. The estimated value of τ by the one-dimensional solutions without the correction factors is only 30 $\sim$ 70 % of the real value derived by the three-dimensional solution.

Experimental results in p- and n-type Si Schottky diodes showed good agreement with the theory, and the minority carrier diffusion constants of electrons and holes were determined as 19 and 7 cm^2/sec, respectively.

References

[1] P. D. Dapkus, W. H. Hackett Jr., O. G. Lorimor and R. Z. Bachrach: J. Appl. Phys. 45 , 4920 (1974)

[2] M. Boulou and D. Bois: J. Appl. Phys. 48 , 4713 (1977)

[3] M. Ettenberg, H. Kressel and S. L. Gilbert: J. Appl. Phys. 44 , 827 (1973)

[4] S. Wang: " Solid-State Electronics " (McGraw-Hill, Inc. 1966) p.300

[5] W. Zimmermann: phys. stat. sol. (a) 12 , 671 (1972)

[6] D. R. Hunter, D. H. Paxman, M. Burgess and G.R. Booker: " Scanning Electron Microscopy: Systems and Applications 1973 " (Inst. Phys. London)pp.208 - 213

[7] H. K. Kuiken: Solid-State Electron. 19 , 447 (1976)

[8] A. Jakubowicz: Solid-State Electron. 23 , 635 (1980)

[9] H. T. Weaver and R. D. Nasby: Solid-State Electron. 22 , 687 (1979)

[10] D. L. Lile and N. M. Davis: Solid-State Electron. 18 , 699 (1975)

[11] W. van Roosbroeck: J. Appl. Phys. 26 , 380 (1955)

[12] W. H. Hackett, Jr. : J. Appl. Phys. 43 , 1649 (1972)

[13] F. Berz and H. K. Kuiken: Solid-State Electron. 19 , 437 (1976)

[14] C. van Opdorp: Philips Res. Rept. 32 , 192 (1977)

[15] D. B. Wittry and D. F. Kyser: J. Appl. Phys. 36 ,1387 (1965)

[16] C. van Opdorp, R. C. Peters and M. Klerk: Appl. Phys.Lett. 24 , 125 (1974)

[17] C. J. Hwang: J. Appl. Phys. 42 , 4408 (1971)

[18] H. Reichl and H. Bernt: Solid-State Electron. 18 , 453 (1975)

[19] G. Schwab, H. Bernt and H. Reichl: Solid-State Electron. 20 , 91 (1977)

[20] J. Müller, H. Bernt and H. Reichl: Solid-State Electron. 21 , 999 (1978)

[21] J. Müller, H. Reichl and H. Bernt: Solid-State Electron. 22 , 257 (1979)

[22] C. Munakata and T. E. Everhart: Jpn. J. Appl. Phys. 11 , 913 (1972)

[23] S. Othmer: " Scanning Electron Microscopy /1978/ Vol.I " (SEM. Inc. O'Hare, Ill.) p.727

[24] J. D. Kamm and H. Bernt: Solid-State Electron. 21 , 957 (1978)

[25] J. D. Kamm: " Semiconductor Silicon 1977 " (The Electrochemical Society, Inc.) p.491

[26] O. von Roos: Solid-State Electron. 23 , 177 (1980)

[27] O. von Roos: J. Appl. Phys. 50 , 3738 (1979)

[28] K. Kanaya and S. Okayama: J. Phys. D: Appl. Phys. 5 , 43 (1972)

[29] J. P. Mckelvey: " Solid State and Semiconductor Physics " (Harper and Row, New York, 1966) pp.439-440

[30] H. F. Wolf:" Silicon Semiconductor Data " (Pergamon Press Inc., 1969)

VII. HEAT TREATMENT EFFECT ON DIFFUSION LENGTH IN Si

7-1. Introduction

There have been many studies [1] on the properties of the process induced faults (PIF's). The degradation of the electrical performance of the devices has much connection with the segregated impurities at PIF's or the decorated faults of each PIF. Recently, the fault produced especially by the oxidation at high temperatures (i.e. so called oxidation induced stacking fault (OSF)) has received considerable attention [2-5] because the oxidation is a fundamental process in making LSI's or charge-coupled devices (CCD's). Ravi et al. [6,7] showed that the electrically active OSF's increased the leakage current in p-n junctions. Kimerling [8] determined the energy level of the faults from the electron beam induced current (EBIC) measurements at various temperatures. Generally, the faults become recombination centers, and decrease the lifetime and the diffusion length of minority carriers. Shimizu [9] showed that the lifetime could be controlled preferably by the intrinsic gettering using OSF's. Rozgonyi [10] and Tanikawa [11] reported that the relaxation time of MOS capacitors decreased as the density of OSF increased. But, there have been a little study on the quantitative information of the decrease of the diffusion length after the oxidation process at high temperatures.

In this chapter, we measured the changes of the diffusion length by EBIC method after the heat treatments at high temperature, and showed that the heat treatment for a few minutes could affect the diffusion length at the surface region. The observation of surface faults by chemical etching were also shown.

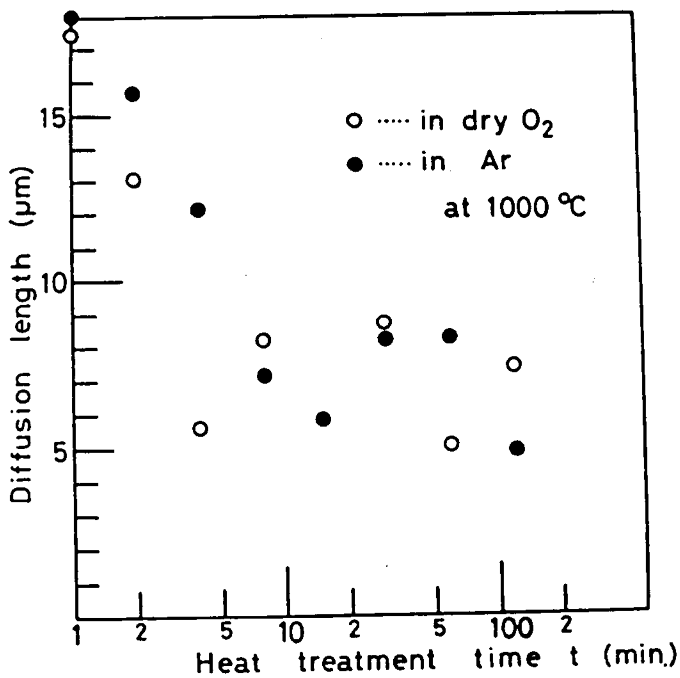

Fig. 7-1 Diffusion length after the heat treatments for various time lengths ranging from 1 to 120 minutes at 1000 °C. Open and solid circles are for the cases in dry O_2 and Ar, respectively. Original diffusion length before annealing is 80 μm.

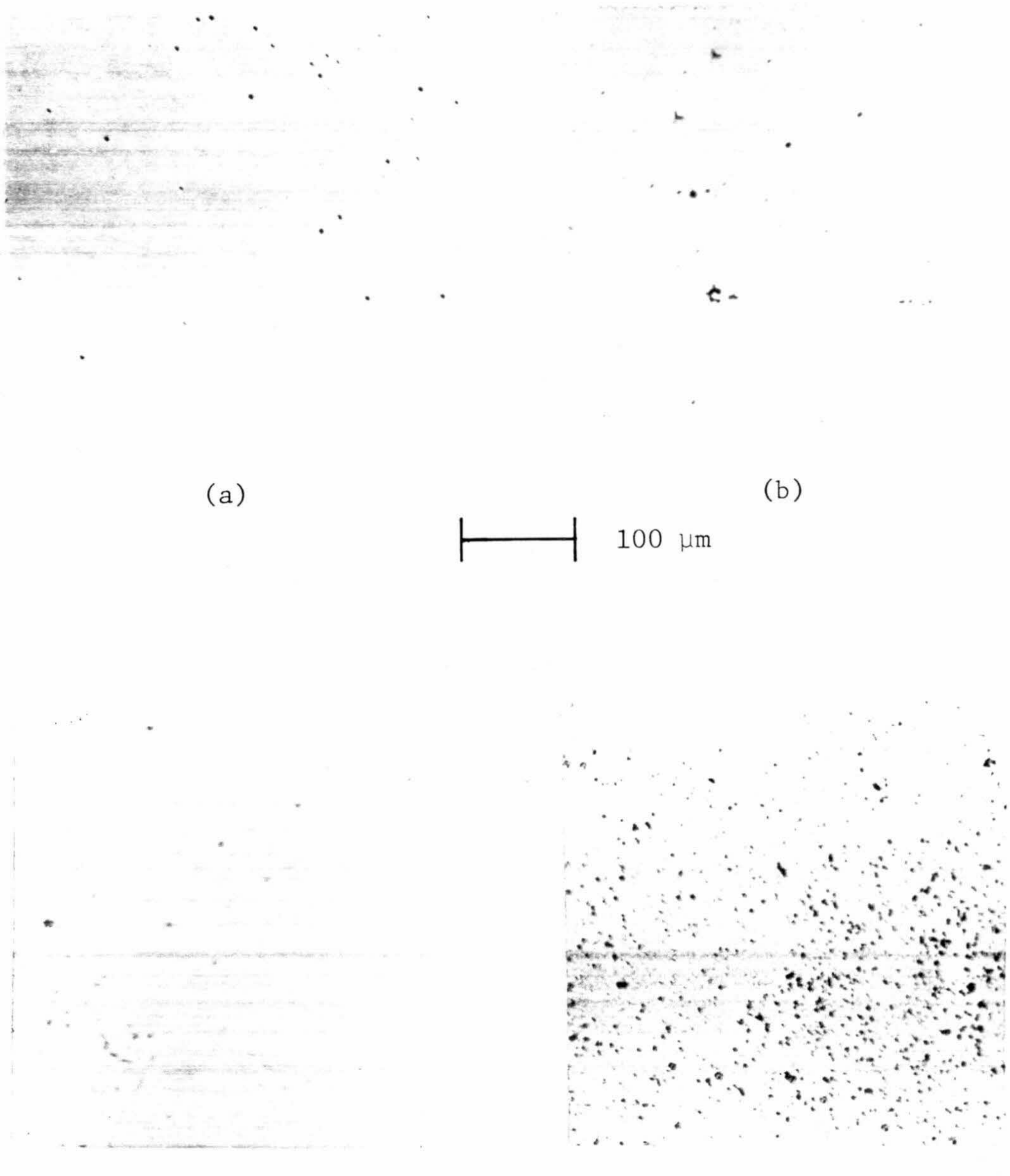

Fig. 7-2 Surface faults revealed by chemical etching using Sirtl etchant. Samples (a), (b), (c) and (d) were annealed in dry O_2 at 1000 °C for 0, 8, 30 and 120 minutes, respectively.

7-2. Experimental results and discussions

Samples are n-type Si grown by CZ method. The original resistivity before annealing is about 0.1 Ωcm. The heat treatment was done at 1000 °C in the flow of dry O_2 and Ar, respectively. Then, the samples were rinsed in HF for 1 min. to remove the oxidized layer, and gold was evaporated in order to make a Schottky barrier for EBIC measurements. The procedures of the determination of the diffusion length have already been discussed in Chapters III, and IV.

Figure 7-1 shows the diffusion length after the heat treatment. The time t of the heat treatment was changed from 1 to 120 minutes. The open and solid circles are for the case in dry O_2 and Ar, respectively. The original value of diffusion length is 80 μm. The diffusion length decreased to about 7 μm rapidly as t increased to 5 min., and became almost constant over the range of $t > 5$ min. The diffusion length decreased slightly more rapidly in O_2 than in Ar. The lifetime changed from 5 μs to 0.03 μs if the diffusion constant of minority carriers was taken as a typical value of 12.5 cm^2/sec. The surface faults of the samples annealed in dry O_2 are shown in Figs. 7-2 (a), (b), (c) and (d) for t= 0, 8, 30 and 120 min., respectively. The samples were etched by Sirtl etchant for the same time. The number of faults did not increase until t=8 min., but became very large at t=120 min. The same result was obtained for the samples annealed in Ar. It should be noted that the number of faults did not changed in the range of $0 \leq t \leq 8$ min., but the diffusion length decreased rapidly in the same range. The lengths between the faults are very large in comparison with the diffusion length in the samples annealed for $1 < t < 8$ min., and so, the diffusion length is considered not to be restricted by the average interval between the faults when the faults are considered to be the carrier sink.

The uniform EBIC was obtained when the electron beam was scanned on the surface through the Schottky barriers, and the dark points corresponding to the faults were not observed.

The rapid decrease of the diffusion length was considered to be caused by the formation of nuclei of faults at the early stage of the heat treatment. The very small nuclei can become the recombination centers even if they cannot be revealed by chemical etching. If the heat treatment time is sufficiently long, the nuclei become large and can be revealed by etching. As shown in Fig. 7-2 (d), the length between the faults after long time heat treatment is the same order of the diffusion length. The formation of nuclei was not affected very much by the oxidation because the decrease of the diffusion length was also observed in the heat treatment in Ar. As is known generally, the CZ grown Si contains oversaturated oxygen, and the formation of nuclei is related to the oxygen precipitation [12]. The diffusion length decreased less rapidly in Ar than in O_2. One reason of this phenomenon is considered to be the formation of SiO_2. Another reason is the outdiffusion of oxygen, because oxygen can outdiffuse more rapidly in Ar than in O_2. Further investigation must be needed for the clarification of the nuclei formation.

In conclusion, the diffusion length at the surface region in Si decreased to about 10 % of the original value after the very short heat treatment at 1000 °C for a few minutes. Nevertheless, the surface faults revealed by chemical etching did not change. The nuclei of faults were considered to be formed at the early stage of heat treatment, and they became minority carrier recombination centers. The decrease of the diffusion length was not so affected by the ambient gases (i.e. oxygen or inert one). Much attention must be payed in the heat treatment process at high temperature even if the time is very short.

References

[1] H. Foll, N. Gorele and B. O. Kolbesen: " Semiconductor Silicon 1977 " (J. Electrochemical Society Inc., Princetion 1977) pp.565-574

[2] D. J. D. Thomas: phys. stat. sol. 3 , 2261 (1963)

[3] C. M. Melliar-Smith: " Crystal defects in silicon integrated circuits — Their cause and effect " in " Treaties on Material Science and Technology" vol. 11 (Academic Press, New York, 1977)

[4] K. V. Ravi and C. J. Varker: J. Appl. Phys. 45 , 263 (1974)

[5] S. M. Hu: J. Appl. Phys. 51 , 3666 (1980)

[6] K. V. Ravi, C. J. Varker and C. E. Volk: J. Electrochem. Soc. 120 , 533 (1973)

[7] C. J. Varker and K. V. Ravi: J. Appl. Phys. 45 , 272 (1974)

[8] L. C. Kimerling, H. J. Leamy and J. R. Patel: Appl. Phys. Lett. 30 , 217 (1977)

[9] H. Shimizu, A. Yoshinaka and Y. Sugita: Jpn. J. Appl. Phys. 17 , 767 (1978)

[10] G. A. Rozgonyi and R. A. Kushner: J. Electrochem. Soc. 123 , 570 (1976)

[11] K. Tanikawa, Y. Ito and H. Sei: Appl. Phys. Lett. 28 , 285 (1976)

[12] J. R. Patel: " Semiconductor Silicon 1977 " (The Electrochemical Society Inc., Princeton, 1977) pp.521-545

VIII. CONCLUSIONS

In the present study, EBIC was analyzed quantitatively by solving the steady-state or time-dependent three-dimensional diffusion equations. The influence of the finite generation volume on EBIC was discussed, and an improved method to characterize the physical properties in the small selected areas of semiconductors was suggested. The obtained results were as follows.

In Chapter II, the short diffusion length of the order of μm could be determined by the normal incidence method of EBIC. Various models for generation distribution used in the analysis yielded the ambiguity for the determination of the diffusion length and the electron-hole pair creation energy by an electron beam. Detailed information on the generation distribution must be necessary to analyze EBIC accurately.

In Chapter III, the generation volume of minority carriers had a considerable effect on EBIC in the line scan method, especially when the dimensions of the generation volume was equal to or larger than the diffusion length. When the accelerating voltage was low, and so, the generation depth was shallow, surface recombination had a large effect on EBIC. Whereas, when the accelerating voltage was high, and so, the generation depth was as large as the diffusion length, surface recombination had a slight effect on EBIC. The accurate values of physical parameters such as the diffusion length should be determined by fitting the experimental data to the theoretical curves for all the accelerating voltages. The existence of a maximum in EBIC near the barrier could be explained by the 'edge effect' attributed to the finite generation volume.

In Chapter IV , in the line scan method, the dependence of EBIC on the scanning distance represented mainly the lateral extent of the generation distribution when the accelerating voltage was high, and when the dimensions of the generation region were larger than the diffusion length. The three-dimensional generation distribution based upon the experimental results for the normal incidence could explain the experimental results of the line scan method. In GaAs, the center of the generation region was located at the point of 0.13 of the maximum electron range, and the radial distribution from the center was shown to be Gaussian with an exponent of $5.4\sim8.2$. The values of $3.8\sim4.4$ eV for the electron-hole pair creation energy by an electron beam was obtained taking the surface recombination effect into account.

In Chapter V, in the line scan method, the minority carrier distribution was affected very much by an ohmic contact when the length w between the potential barrier and the ohmic contact was less than one or two diffusion lengths. The slope of the curve of EBIC vs. scanning distance did not change even when the diffusion length varied, and the diffusion length could not be determined definitely from the slope of the curve. The absolute value of EBIC was dependent on the surface recombination velocity and the length w.

In Chapter VI , the phase shift between the modulated electron beam and EBIC was clarified by solving the three-dimensional time-dependent diffusion equation. The relation between the phase shift and the lifetime was found to be expressed using the approximated solutions of the one-dimensional diffusion equation with empirical correction factors. The lifetime and the diffusion constant of minority carriers could be determined definitely without any restriction for modulation frequency.

In Chapter VII, the diffusion length in the surface region of Si was found to be decreased very much after heat treatment at 1000 °C for only a few minutes , nevertheless surface faults revealed by chemical etching were not increased. The nuclei of the faults might be formed at the early stage of heat treatment.

This investigation proved that EBIC could be analyzed quantitatively in the small selected area considering the three-dimensional generation distribution by an electron beam. But, there exist some points to be studied further as follows. First, by EBIC method, the total recombination lifetime including both radiative and non-radiative processes can be measured. But, one cannot observe the radiative recombination lifetime alone which is the important parameter to characterize the light-emitting diodes or laser diodes [1] . Deeper understanding can be acquired by investigating the luminescence emitted by recombination of generated electron-hole pairs (i.e. cathodoluminescence) [2,3]. Secondly, EBIC technique cannot reveal the energy levels and densities of impurities and traps accurately which affect the electrical properties of materials very much. There have been a few reports [4] to determine the energy levels of faults in Si from EBIC measurements at various temperatures. But, the experimental accuracy of EBIC technique is inferior to that of the photoluminescence [5] or the capacitance [6,7] methods. Thirdly, the dose of high energy electron beam causes damages in samples. Several investigations have shown the decrease of the threshold voltage in MOS devices [8] and the increase of the interface state density between the oxide and the semiconductors[9].

Improvements of measurement techniques (i.e. use of the low energy primary electron beam , or the decrease of the total amount of dose) will be necessary.

Electrical properties of semiconductors can be characterized collectively by EBIC jointly with the other techniques which complement the weak points in EBIC method.

REFERENCES

[1] P. D. Dapkus, W. H. Hackett, Jr., O. G. Lorimor and R. Z. Bachrach: J. Appl. Phys. 45 , 4920 (1974)

[2] D. B. Holt and B. D. Chase: phys. stat. sol. (a) 20 , 135 (1973)

[3] M. Boulou and D. Bois: J. Appl. Phys. 48 , 4713 (1977)

[4] L. C. Kimerling, H. J. Leamy and J. R. Patel: Appl. Phys. Lett. 30 , 217 (1977)

[5] H. Barry Bebb and E. W. Williams: "Semiconductors and Semimetals" (ed. R. K. Willardson and A. C. Beer, Academic Press, 1972) vol. 8 pp. 182-392

[6] S. M. Sze: "Physics of Semiconductor Devices" (John Wiley & Sons, Inc. 1969)

[7] D. V. Lang: J. Appl. Phys. 45 , 3023 (1974)

[8] W. J. Keery, K. O. Leedy and K. F. Galloway:" Scanning Electron Microscopy /1976/ " (IITRI, Chicago) pp.507-514

[9] R. Hezel: Solid-State Electron. 22 , 735 (1979)

LIST OF PUBLICATIONS

I. Papers

[1] " The influence of the generation volume of minority carriers on EBIC "
T. Fuyuki , H. Matsunami and T. Tanaka
J. Phys. D: Appl. Phys. 13 , 1093-1100 (1980)

[2] " Analysis of EBIC considering the generation distribution of minority carriers "
T. Fuyuki , H. Matsunami and T. Tanaka
J. Phys. D: Appl. Phys. 13 , 1503-1510 (1980)

[3] " Determination of lifetime and diffusion constant of minority carriers by a phase shift technique using electron beam induced current "
T. Fuyuki and H. Matsunami
J. Appl. Phys. 52 , (1981)

[4] " Analysis of electron beam induced current considering sample dimensions — Measurement of diffusion length and surface recombination velocity — "
T. Fuyuki and H. Matsunami
Jpn. J. Appl. Phys. 20 , (1981) No.4

[5] " Influence of minority carrier generation distribution on electron beam induced current in the normal incidence method "
T. Fuyuki and H. Matsunami
(to be published)

[6] " Heat treatment effect on diffusion length in Si "
T. Fuyuki and H. Matsunami
(to be published)

II . Publications in the Institute of Electronics and Communication Engineers of Japan

(in Japanese)

[1] " Measurement of minority carrier diffusion length by EBIC method "
T. Fuyuki, H. Matsunami and T. Tanaka
Rept. Tech. SSD 78-102 (Feb. 1979)

[2] " Characterization of diffusion length and lifetime by EBIC "
T. Fuyuki and H. Matsunami
Rept. Tech. SSD 79-103 (Feb. 1980)

[3] " Measurement of lifetime and diffusion constant of minority carriers by phase shift technique in EBIC "
T. Fuyuki and H. Matsunami
Trans. Section J63-C , 832-837 (1980)